Nanoscale Advances

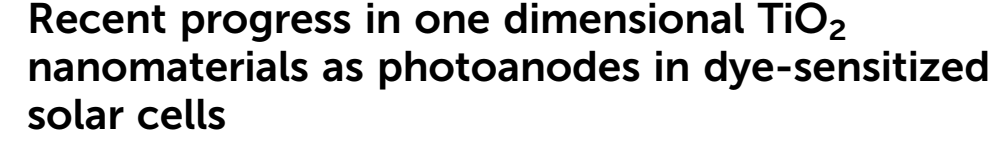


REVIEW

View Article Online



Cite this: Nanoscale Adv., 2022, 4,



Deepak Joshy, a Soumya B. Narendranath, b Yahya A. Ismail a and Pradeepan Periyat (1)*c

Exploiting the vast possibilities of crystal and electronic structural modifications in TiO₂ based nanomaterials creatively attracted the scientific community to various energy applications. A dye sensitised solar cell, which converts photons into electricity, is considered a viable solution for the generation of electricity. TiO₂ nanomaterials were well accepted as photoanode materials in dye-sensitized solar cells, and possess non-toxicity, high surface area, high electron transport rates, fine tuneable band gap, high resistance to photo corrosion and optimum pore size for better diffusion of dye and electrolyte. This review focuses on various aspects of TiO2 nanomaterials as photoanodes in dye-sensitized solar cells. TiO₂ photoanode modification via doping and morphological variations were discussed in detail. The impact of various morphologies on the design of TiO₂ photoanodes was particularly stressed.

Received 6th July 2022 Accepted 26th September 2022

DOI: 10.1039/d2na00437b

rsc.li/nanoscale-advances

Introduction

The excessive consumption of fossil fuels to meet the increasing energy demand has resulted in profound consequences such as global warming, environmental pollution, etc. To address the challenges raised by environmental degradation and the energy crisis, the development of a sustainable energy production

approach is required. Even though various renewable energy resources such as geothermal energy, biofuels, and wind-tidal energies can substantially contribute to sustainable energy development, solar energy has to play a major role. In this era of growing energy demand and environmental issues, solar energy is the only choice left in front of us as solar radiation possesses immense potential, vast abundance and environmental friendliness. Out of the 4 million exajoules (10¹⁸ J) of solar energy reaching the earth, around 50 000 EJ's are easily exploitable.1 The significance of solar energy becomes more clear from the fact that the world's annual energy consumption

Department of Environmental Studies, Kannur University, Kerala, India. E-mail: pperiyat@kannuruniv.ac.in



Mr Deepak Joshy is presently working as a Senior Research Fellow under the CSIR-UGC JRF scheme in the Department of Chemistry, University of Calicut under the guidance of Dr Pradeepan Periyat. His research mainly focuses on the design and development of nanomaterials for energy saving and environmental applications. His major research areas are photocatalysts and adsorbents for

water purification, inorganic pigments for cool coatings and supercapacitors.



Dr Soumya B. Narendranath is currently a post-doctoral fellow in the Department of Chemistry, Central University of Kerala, India. She obtained her PhD degree from CSIR-National Chemical Laboratory (NCL), Pune, where she studied photocatalytic water splitting activity of layered metal oxides. She is the recipient of the SERB-National Post-Doctoral Fellowship and Dr D. S. Kothari-UGC

Fellowship. She has completed two post-doctoral fellowships at Central University of Kerala. Her research interests include design and development of metal oxide nanoparticles for solar energy utilization and heterogeneous catalysis for biomass conversion.

^aDepartment of Chemistry, University of Calicut, Kerala, 673635, India

^bDepartment of Chemistry, Central University of Kerala, 671316, India

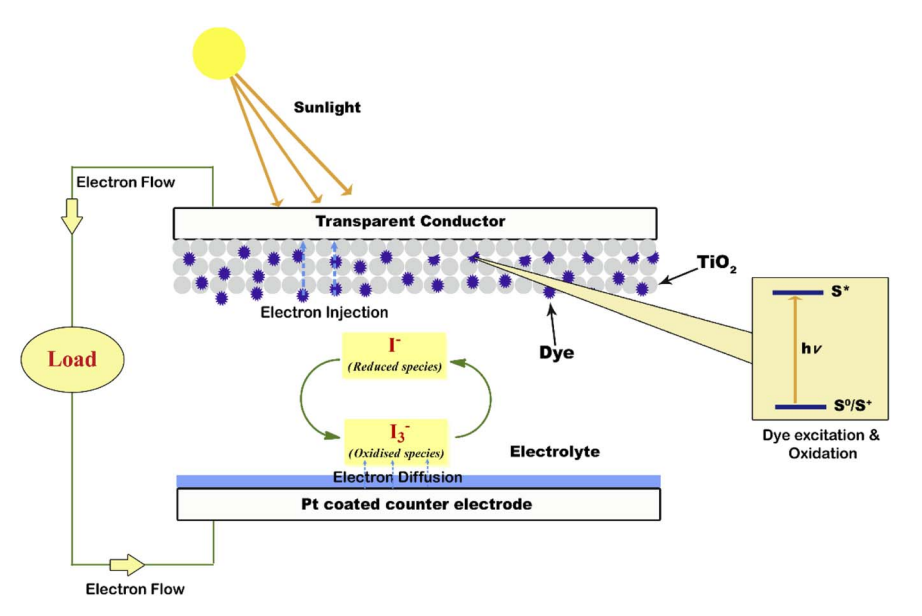


Fig. 1 Schematic diagram of a DSSC.

for the year 2017 was around 565 EJ's which is only a fraction of the harvestable solar energy (i.e. 50 000 EJ's).² But in the present scenario, electricity produced from the renewable energy sector constitutes only 8.4% of the total world electricity production.² More than 20% of the contribution to the renewable energy sector is made by solar energy.3 But this share of solar energy is significantly small compared to the magnitude of solar power available for harvesting. The lack of efficient and economically viable solar harvesting techniques is the main reason for this huge difference. Solar cells are one of the widely employed solar energy conversion devices. Solar cells are classified into different generations based on the material and technology present in them. We have first generation silicon solar cells as the most widely commercialized solar cell type. 4,5 Silicon solar

cells have efficiencies of around 26% which is almost near the theoretical efficiency maximum.⁶ At the same time, secondgeneration solar cells are based on thin-film technology and employ materials such as CdTe, CIGS, etc.7-10 The efficiency of second-generation solar cells has reached up to 21.7% recently.6 But the large-scale commercialization of first and secondgeneration solar cells is very expensive. Also, the components used in these two generations are capable of causing environmental hazards. So, to develop an economically viable and ecofriendly way of solar energy conversion, the third generation of solar cells, known as dye-sensitized solar cells (DSSCs) was introduced.11-14 The concept of a DSSC was introduced by Michael Gratzel in 1991.15 Significant attraction garnered by DSSCs is due to their large-scale and economically viable



Dr Yahya A. Ismail received his PhD from Aligarh Muslim University (AMU), India. He joined as a Reader in Chemistry at University of Calicut in 2005. Then he worked as a CRI researcher at the Center for Bio artificial Muscles, Hanyang University, South Korea. Later, he served as a faculty member in University of Nizwa and Al Sharqiyah University, Oman. Presently, he is working as an

Associate Professor of Chemistry, University of Calicut, India. His research is focused on conducting polymer-based artificial muscles and sensors, electrochemical super capacitors and stimuli responsive polymers.



DrPradeepan Periyat currently working as an Associate Professor and Head, Department of Environmental Studies, Mangattuparamba Campus, Kannur University, Kerala, India. He completed two post doctoral fellowships at University of Limerick, Ireland and Monash University, Mel-Australia. He was bourne. awarded the prestigious Marie-Curie Fellowship from 2009 to

2012. He is an Associate Member of the Royal Society of Chemistry (RSC), London. He received the Young Scientist Award 2017 from KSCSTE, Kerala State Government. He has published 60 scientific articles in leading peer reviewed journals and 12 book chapters. His research group focuses on nanomaterials synthesis for energy and environmental applications.

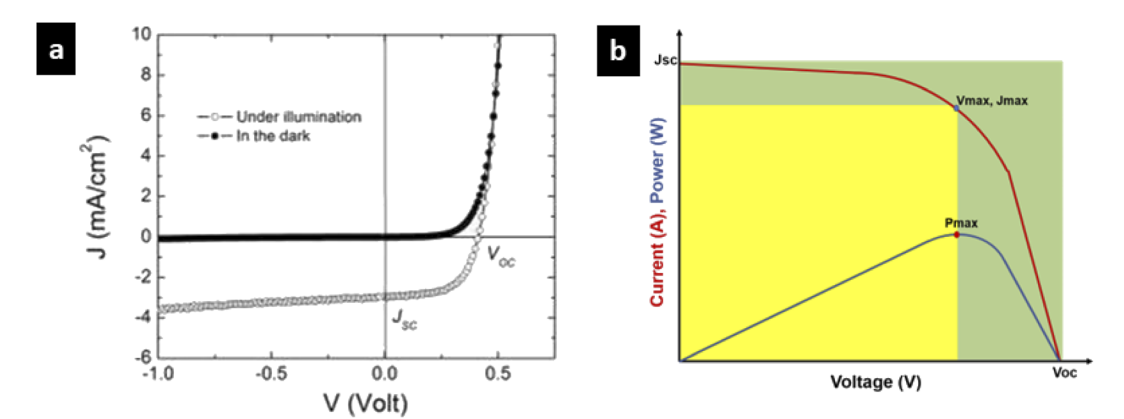


Fig. 2 (a) The current *versus* voltage curve associated with a solar cell circuit in the dark and under illumination (Copyright: https://depts.washington.edu/). (b) Graphical representation of the fill factor.

production capability along with flexibility. The efficiencies of DSSCs introduced so far are found to be within 14.3%. 16 If the issues associated with low efficiency and shorter durability are addressed properly, DSSCs are the best to play a vital role in the development of a sustainable energy culture. Also, large-scale commercialization of DSSCs can convert a major share of the available solar radiation. Performance enhancement, durability increment and production cost reduction of DSSCs can be carried out in various ways. Mainly it involves either the synthesis of novel component materials/modification of existing materials or the introduction of more rational DSSC designs. As a DSSC assembly consists of various components such as a photoanode, sensitizer(dye), counter electrode, redox electrolyte, etc., investigation into performance enhancement can be carried out on any one of these components. In this review, special emphasis is given to the DSSC photoanode and the contribution of one dimensional TiO2 nanomaterial based photoanodes for the critical development of DSSCs.

1.1. DSSC structure & working- an overview

A photoanode forms the core part of the DSSC and it consists of a transparent conducting oxide (TCO) glass plate or plastic substrate on which nanometre-sized semiconducting metal oxide particles are deposited and sintered. Fluorine-doped tin oxide (FTO) is the most widely employed substrate. 17,18 Usually, a mesoporous TiO₂ film having a thickness of around 10 μm is coated on the FTO substrate to facilitate electron transfer.19 Sensitizer or dye molecules responsible for light absorption are adsorbed onto the mesoporous nanomaterial film. Upon irradiation by solar radiation, the dye molecule will get excited and emit an electron. This emitted electron will get injected into the conduction band of the nanocrystalline semiconductor metal oxide film. From there the electron will get transferred to the FTO plate and then to the external circuit. The dye molecule which got oxidised on solar irradiation is now regenerated by employing a redox couple. 20,21 The iodide/triiodide redox system is the most widely used one.²² Upon reduction of the oxidised dye molecule, the iodide ion gets oxidised into triiodide. The regeneration of the redox couple is facilitated by electrons

which reach the counter electrode through the external circuit. The counter electrode consists of a thin layer of Pt nanoparticles deposited on a conducting glass substrate.23,24 Here the electron emitted from the dye molecule travels through the mesoporous nanomaterial layer deposited on the FTO plate and then flows through the external load and finally reaches the counter electrode to regenerate the redox system. The redox electrolyte system present in between the two electrodes not only facilitates dye regeneration but also prevents the recombination of conduction band electrons with oxidised dye molecules. While fabricating the DSSC, as shown in Fig. 1 the photoanode and cathode are sandwiched together with a layer of the polymer film in between them.25 Then the redox electrolyte system is injected into the space in between so that the triiodide ions can diffuse towards the counter electrode and get reduced to iodide ions. A number of such repeating cycles produce current in the circuit. The resultant efficiency of a DSSC depends on the electron recombination rate. The lower the electron recombination rate, the higher the efficiency will be. The lower electron recombination rate results from the high electron transport rate.26

1.2. Important terms associated with DSSCs

The important parameters associated with dye sensitised solar cells are incident photon-to-current efficiency (IPCE), open circuit voltage ($V_{\rm OC}$), short circuit current ($J_{\rm sc}$), fill factor (FF) and cell efficiency.

1.2.1 Short circuit photocurrent ($J_{\rm sc}$). Fig. 2a shows the current *versus* voltage curve associated with a solar cell circuit in the dark and under illumination. When the electrons travel from the anode to the cathode of the solar cell, and on the other hand when the circuit is reverse biased, the current flows will be zero. This is due to the hindrance caused by the high energy barrier of the donor. After the energy barrier is crossed, a very low current will flow. This feature is represented by the dark curve. When the solar radiation is absorbed by the donor, charge carriers will be generated easily. There will be a reverse current due to the electron flow from the anode to cathode. This reverse current which has resulted in

the absence of an external voltage is termed as photocurrent or short circuit photocurrent (J_{sc}) . This is represented by the hollow bubbled curve.

- 1.2.2 Open circuit voltage (V_{OC}) . Since the short circuit current is a result of the reverse bias current, it is possible to compensate the current by applying a forward voltage. Under this condition, there will be a point where the current becomes zero. The voltage corresponding to this point is referred to as the open circuit voltage (Voc). On the other hand, the open circuit voltage is the maximum voltage available from a solar cell when there is no external load connected and the external current flowing through the cell is zero.27
- 1.2.3 Fill factor (FF). The solar cell fill factor (FF) gives us an idea of the performance of the solar cell.28 It corresponds to the ratio of the actual performance to the theoretical maximum power output of a solar cell.

$$FF = \frac{J_{\text{max}} \times V_{\text{max}}}{J_{\text{sc}} \times V_{\text{oc}}}$$

A higher fill factor favours the maximum output of a solar cell. The graphical representation of the fill factor is shown in Fig. 2b. This graph shows the solar cell output current and power as a function of voltage. It is the ratio of the area of the larger rectangle (pale green) to the area of the smaller rectangle (yellow).

- 1.2.4 Incident photon-to-current efficiency (IPCE). The incident photon-to-current efficiency (IPCE) is a measure of the ratio of the photocurrent (converted to an electron transfer rate) vs. the rate of incident photons (converted from the calibrated power of a light source) as a function of wavelength.29 IPCE is also known as quantum efficiency which measures the efficiency of a device to convert incident photons into electrical energy at a given wavelength.
- 1.2.5 Solar cell efficiency. The efficiency of a solar cell is defined as the fraction of incident solar power which is converted to electricity. Solar cell efficiency depends on the spectrum, intensity of incident sunlight and the temperature of the solar cell. Therefore, conditions under which efficiency is measured must be carefully controlled to compare the performance of one device to that of another one.30 Terrestrial solar cells are measured under AM1.5 conditions and at a temperature of 25 °C. The maximum output power is given by

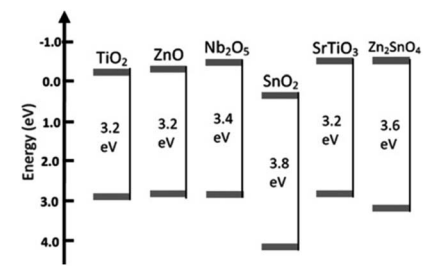


Fig. 3 Band positions of various semiconductor oxide materials used as photoanodes.⁵⁷ (Reprinted with permission from ref. Yang et al., 2013. Copyright 2013 WILEY-VCH Verlag GmbH & Co. KGaA, Weinheim.)

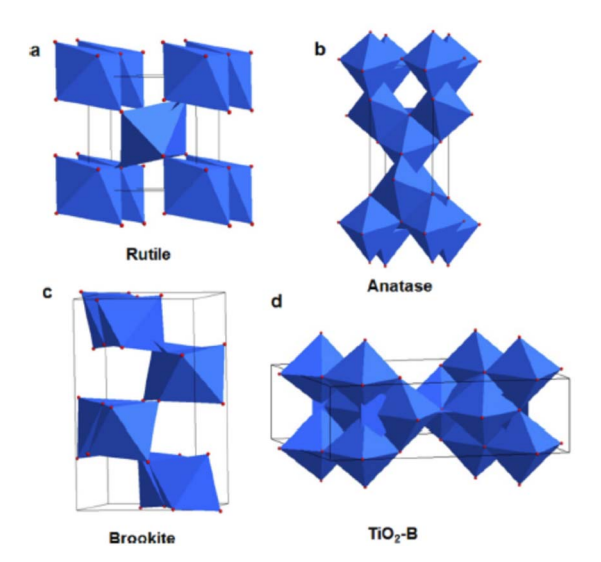


Fig. 4 Schematic unit cell structure of four TiO₂ polymorphs: (a) rutile (b) anatase (c) brookite and (d) TiO₂ (B)⁶⁶ (Reprinted with permission from ref. Wang, X. et al., 2014. Copyright 2014 American Chemical Society).

$$P_{\rm max} = V_{\rm oc} \times J_{\rm sc} \times {\rm FF}$$

Then efficiency is given by the equation,

$$\eta = V_{\rm oc} \times J_{\rm sc} \times FF/P_{\rm in}$$

where $V_{\rm OC}$ is the open circuit voltage, $J_{\rm SC}$ is the short circuit current and FF is the fill factor.11

1.3. Role of the photoanode in a DSSC

Among the functional components of a DSSC, the photoanode forms the crucial part. The nature of the material used as the photoanode and its morphology are important factors determining the overall performance of a DSSC. The functions of a photoanode include dye pickup, electron injection, transportation and collection which in turn influence the photocurrent, photovoltage and power conversion efficiency. Efforts are being made to improve the efficiency of DSSCs by introducing novel materials as photoanodes and by modifying the morphologies of existing materials. The essential requirements for an ideal photoanode are:

- (i) Higher surface area facilitates the adsorption of dye molecules to a greater extent.31,32
- (ii) Photoanodes should have higher electron transport rates so that the electron injection from the dye to the external circuit through the photoanode occurs smoothly.33
- (iii) Photoanodes should have suitable band gap alignment with the energy levels of the sensitizer.34
 - (iv) It should possess high resistance to photo corrosion.³⁵
- (v) Photoanode materials should possess a pore size that can be optimized to achieve better diffusion of dye and electrolyte.³⁶
- (vi) It should possess the ability to absorb/scatter sunlight for the improved performance of the dye.37

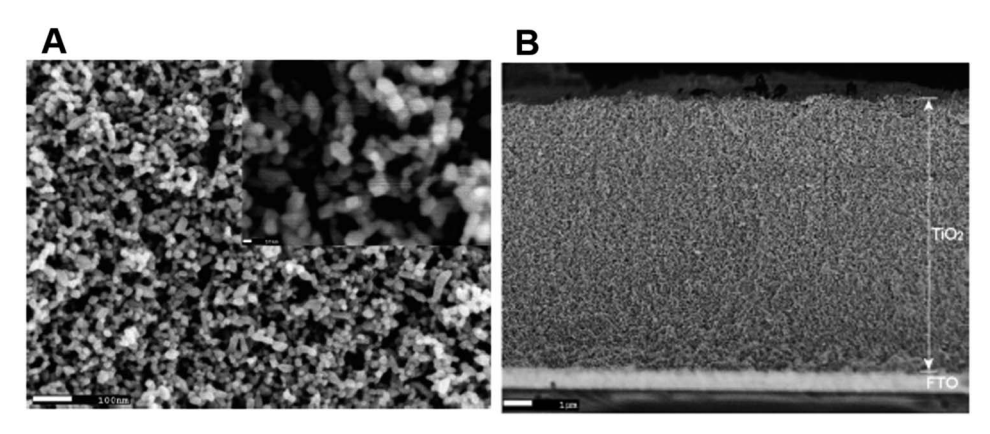


Fig. 5 (a) SEM images of mesoporous TiO_2 and (b) film thickness of mesoporous TiO_2^{73} (Reprinted with permission from ref. Muniz *et al.*, 2011. Copyright 2010 Elsevier).

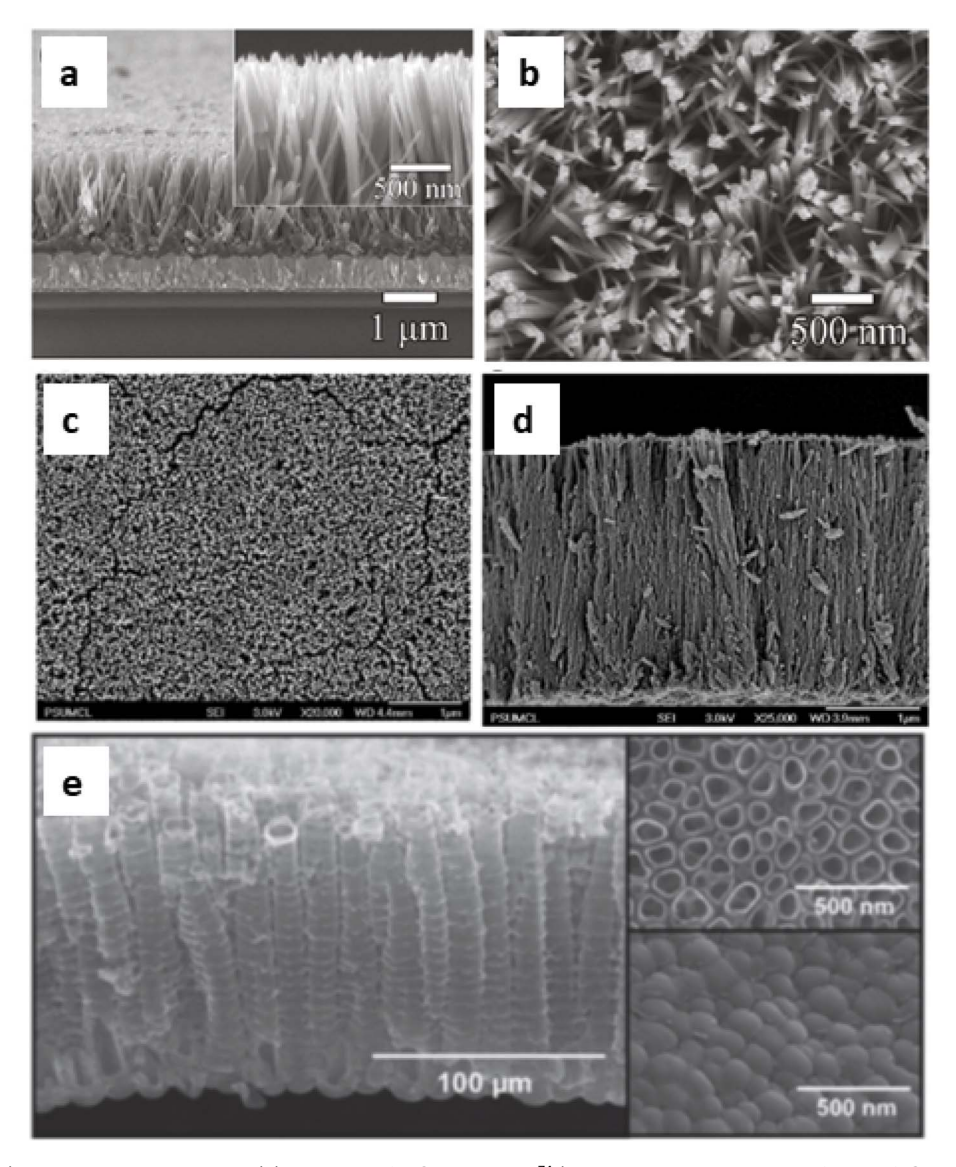


Fig. 6 SEM images: (a) cross sectional view and (b) top view of TiO_2 nanorods⁷⁴ (Reprinted with permission from ref. Cho *et al.*, 2011. Copyright 2011 American Chemical Society); FESEM images (c) top view images and (d) cross sectional image of a TiO_2 nanowire array on FTO coated glass⁷⁵ (Reprinted with permission from ref. Feng *et al.*, 2008. Copyright 2008 American Chemical Society) and (e) SEM images of TiO_2 nanotubes⁷⁶ (Reprinted with permission from ref. Roy *et al.*, 2010. Copyright 2009 Royal Society of Chemistry).

Review Nanoscale Advances

(vii) The photoanode material needs to be in optimum contact with the dye molecules and the conducting substrate.38

The above-mentioned characteristics are vital in achieving a better photoconversion efficiency.

This review discusses the significance of TiO₂ nanomaterials as photoanodes in DSSCs. The characteristic photovoltaic properties and important modifications of TiO2 for photoanode applications are surveyed. A summary of research on TiO₂ and its important one-dimensional morphologies and their modifications to be used as photoanode materials in DSSCs is given here.

2. Photoanode materials

The limitations associated with the conventional materials lead to the investigation of more effective photoanode materials, which have advanced properties with bulk and surface modifications. Commonly investigated materials include metal oxides such as TiO_2 , ZnO_3^{9-42} Nb_2O_5 , $^{43-45}$ SnO_2 , $^{46-48}$ $SrTiO_3$, 49,50 WO_3 , $^{51-53}$ and Zn₂SnO₄.54-56 All these are wide band gap semiconductor materials whose structure, morphology and crystallinity decide the performance of the DSSCs. The band structures of these materials are shown in Fig. 3.57

Among these materials, TiO2 and ZnO are the most widely used materials for DSSC fabrication.58-62 Although ZnO has better electron mobility compared to TiO2, its efficiency is less than those DSSCs employing TiO2. This lower efficiency of ZnO emerges due to decreased dye adsorption and instability in acidic environments.63 Therefore, TiO2 has superior photovoltaic applicability compared to ZnO. Four polymorphs of TiO₂ are known, viz, as rutile (tetragonal), anatase (tetragonal), brookite (orthorhombic) and TiO2 (B) (monoclinic) as shown in Fig. 4.64-66 Among these polymorphs of TiO2, anatase is preferred over rutile for photovoltaic applications irrespective of rutile's greater stability and lower band gap. This is because the anatase phase has a higher conduction band energy level, absorptive affinity and a lower electron-hole recombination rate.67 Since the synthesis of brookite TiO2 is difficult, its applicability as a photoanode remains less explored.68

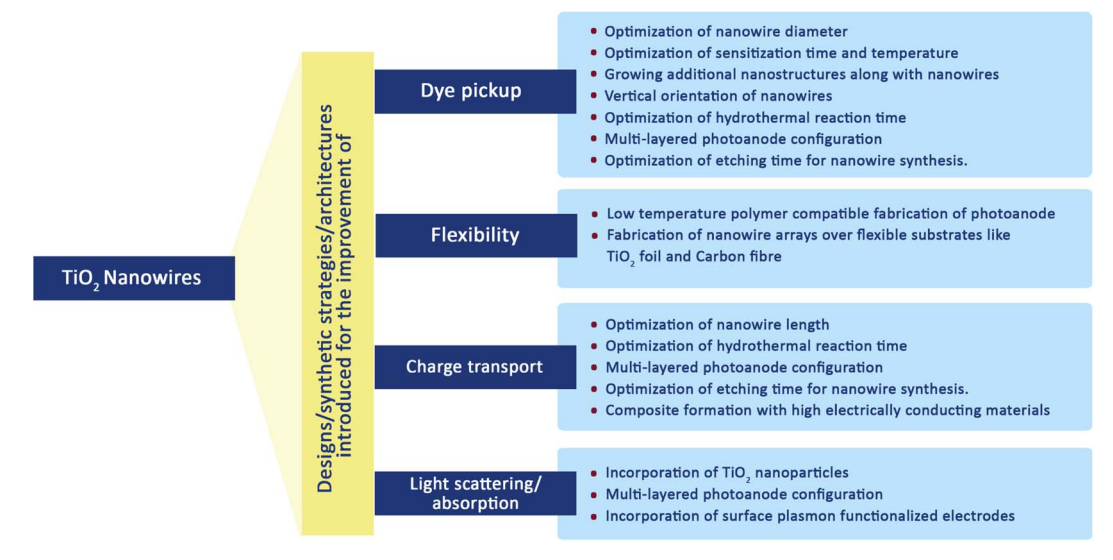
DSSCs employing anatase TiO₂ showed efficiencies ranging from 12-14%. ^{69,70} So TiO₂ is considered the best choice available as a photoanode material due to its (a) cost-effectiveness, (b) easy availability, (c) good stability along with non-toxicity and (d) suitable optical and electronic characteristics.⁶⁷ Furthermore, most of the stable sensitizers showing higher light absorption capability have their LUMO positioned favourably with the conduction band of TiO2. These favourable qualities of TiO₂ initiated further investigations to improve the functioning of TiO₂ photoanodes. During this process of improvement, the main challenges to deal with include the (i) large band gap (3.2 eV) of TiO₂ causing adsorption in the UV region⁷¹ and (ii) low internal electron transport rate.72 Furthermore, research aimed at better performance of TiO₂ by focusing on factors such as high surface area, an increased light scattering effect, enhanced interface quality, fast electron mobility and better charge collection ability. The physical, chemical and optical properties of TiO₂ depend not only on its intrinsic electronic structure but

also on its shape, size, porosity, pore size distribution, organization and surface features. One approach to increase the photoconversion efficiency is by maximising the surface area of TiO₂ and thereby enhancing the reaction at the interface of the photoanode and interacting media. The extent of dye adsorption depends on the surface area available. The greater the dye pickup, the more the electron/current density that will be generated. Semiconductor mesoporous TiO₂ (Fig. 5), nanorods (Fig. 6a and b), nanowires (Fig. 6c and d), nanotubes (Fig. 6e), nanosheets and various other nanoarchitectures have been employed and explored for enhanced dye adsorption.73-76 Besides increasing the surface area, enhancing electron mobility is also a crucial factor in improving the performance of the photoanode. Defects in TiO2 act as electron traps at the grain boundaries and the absence of defects will assure better collection of injected electrons from the semiconductor. Another method involves surface modification of TiO2 semiconductors which has remarkable influence on charge separation, electron mobility and the recombination process.77 Attempts are being made to minimise electron recombination losses due to grain boundaries and also to extend the absorption of TiO₂ towards the near-infrared region.

2.1. TiO₂ photoanode modification by doping

Electronic properties of TiO₂ can be effectively modified by doping i.e. by the deliberate insertion of impurities into the TiO₂ lattice.⁷⁸ Doping in the TiO₂ lattice results in an increase in free charge carriers and conductivity.79 This is due to the defectridden nature of TiO2 and it influences the electronic structure and trap states present in the lattice.80 While doping, either the Ti⁴⁺ cation or O²⁻ anion can be replaced. TiO₂ has a band structure consisting of conduction band (CB) energy levels formed by the Ti⁴⁺ orbitals and valence band (VB) energy levels comprised of O²⁻ 2p orbitals.⁶⁷ Thus replacing Ti⁴⁺ and O²⁻ ions will alter the CB and VB structures respectively.81 The atomic radii of the dopants should be comparable to the ions to be replaced.82 The sensitizer dye molecules used to bind with Ti atoms in the TiO2 lattice and the replacement of Ti with other atoms will affect the dye adsorption due to different binding strengths between the dye and the dopant.83,84 It was also observed that the growth rate of TiO2 nanoparticles is inhibited by dopants resulting in smaller particles having increased surface area.85,86 As a result of an increase in surface area, dye adsorption and current densities are improved.87 This will automatically enhance light absorption and facilitate the use of thinner films having a lower recombination rate in DSSCs.32

Various morphologies of TiO₂ have a major influence on its optical and electronic properties.88 It is found that one-dimensional nanostructures such as nanowires, nanorods and nanotubes possess better charge transport properties compared to nanoparticle assemblies.89 However, these 1D structures have lesser surface area than nanoparticle systems and thereby have reduced dye pick-up capability.90 Dopants having better dye adsorption capacities can improve the photovoltaic performance of 1D nanostructures. 91,92 At the same time, nanoparticle assemblies benefit from dopants that cause increased charge Nanoscale Advances Review



Scheme 1 Various modifications introduced for the improvement of TiO₂ nanowire based DSSC performance.

transfer.⁹³ Hence, it is difficult to identify clearly whether performance improvement is caused by an increase in absorption or electronic effects in doped TiO₂.

Based on the general electronic configuration, dopants can be classified into alkaline earth metals, 94-96 metalloids, 97-99 nonmetals, 100-102 transition metals, 103 post-transition metals 104,105 and lanthanides. 106-108 Significant attempts were made for codoping in which more than one dopant is introduced into the lattice for enhanced device performance. 109-111 Doping in a TiO2 lattice alters its phase, flat band potential, recombination rate, electron transport rate and dye adsorption capability.79 Anatase to rutile phase transformation is inhibited by doping, 112 thereby reducing charge carrier recombination. The flat band potential will experience either a positive or a negative shift i.e. a positive shift involves the downward shift of the CB and Fermi level ($E_{\rm F}$) whereas a negative shift involves the upward shift of the CB and $E_{\rm F}$. A decrease in the number of defect states upon doping increases the lifetime of photogenerated electrons and reduces recombination losses.113 At the same time, a decrease in the number of trap states may lead to enhanced electron mobility.¹¹⁴ Dopants influence the growth rate of nanoparticles, thereby affecting their size, surface area and the number of grain boundaries. Also, dopants decide the binding strength

between the doped surface and dye molecules.¹¹⁵ Recently, Mndoped TiO₂ with IR absorbing capability was reported to be an excellent photoanode for dye-sensitized solar cells and it possesses 79% higher efficiency compared to commercial P25.¹¹⁶

2.2. Nanostructured TiO₂ photoanode

A revolutionary breakthrough in the field of photoanode fabrication with the introduction of a mesoporous TiO₂ nanoparticle photoanode was pioneered by Gratzel and co-workers in 1991.¹¹⁷ They replaced the bulk TiO₂ photoelectrode with a nanostructured architecture and obtained an efficiency of 7.1–7.9% by employing a trimeric Ru complex.¹¹⁸ Detailed guidelines for the fabrication of a TiO₂ nanoelectrode for DSSCs with efficiency >10% are given by Gratzel and team.¹¹⁹ They introduced a double-layered TiO₂ film comprising of a light-absorbing layer of anatase with 20 nm thickness and a light scattering overlayer of 200–400 nm sized anatase particles.¹¹⁹ Soon several multilayered TiO₂ photoanodes were introduced to achieve broadband light confinement without affecting dye adsorption capacity.¹²⁰

Several modifications and novel nanoarchitectures of ${\rm TiO_2}$ have been introduced to exploit the nanoscale properties for

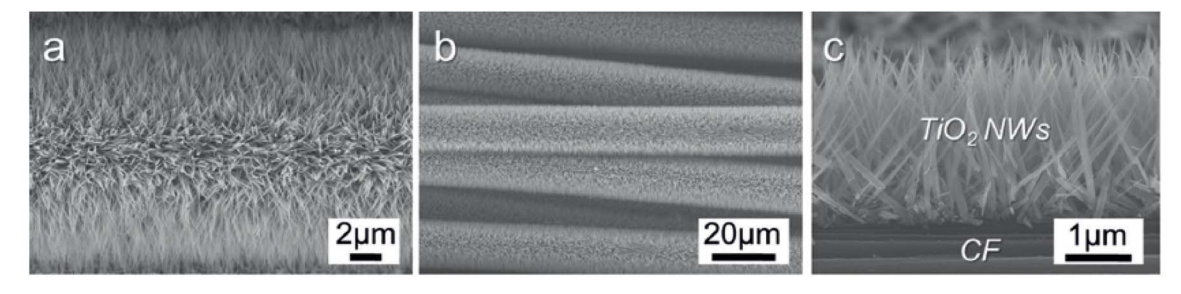


Fig. 7 (a–c) Field emission (FE)-SEM images of TNW arrays grown on a CF substrate at 190 °C for 80 min. (Reprinted with permission from ref. Cai *et al.*, 2014. Copyright 2014 WILEY-VCH Verlag GmbH & Co. KGaA, Weinheim.)

better DSSC performance. 121 Zero dimensional TiO₂ nanoparticles serve as the growth centres for advanced nanoarchitectures with enhanced performance parameters. When the particle size approaches the nanometre range, the nanostructure band gap increases as a result of quantum size effects and it is possible to adjust the valence and conduction band energy levels of the nanosemiconductor with respect to the redox potentials of the redox couple used.

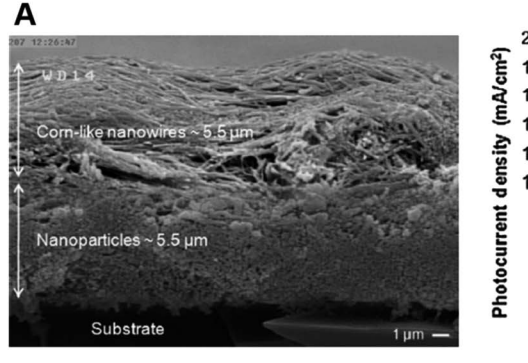
3. One-dimensional nanostructures as photoanodes

One-dimensional nanostructures employed in DSSCs consist of nanotubes, nanowires, nanofibres, nanobelts and nanoribbons. One-dimensional nanomaterials gained attention through the pioneering work by Iijima. A well-ordered arrangement of one-dimensional nanostructures can provide a direct electron transport pathway from the semiconductor film to the conducting substrate. This results in a reduction in the electron recombination rate and an increase in PCE. 123

3.1. Nanowires

TiO₂ nanowire structures serve as confined conducting channels with their long charge diffusion lengths preventing charge recombination and thus facilitating better charge transport.66 It is this fast charge transport and better charge collection ability which made them possible candidates for DSSC fabrication. By using a dense array of long, thin nanowires as dye scaffolds, it is possible to increase both dye pickup and carrier collection efficiency. Also, nanowire photoanodes are found to be more suitable for non-standard electrolytes such as solid inorganic phases or polymer gels having higher recombination rates. 123 Transient photocurrent and photovoltage measurements were carried out on TiO2 nanowires and it was found that the electron transport time and its dependence on illumination intensity are similar to that of TiO₂ nanoparticles. 124 However, the ratio of electron-hole recombination time and electron collection time of TiO2 nanowire-based DSSCs are about 150 times that of nanoparticle-based solar cells and it indicates the improved collection efficiency of nanowire arrays. Scheme 1 gives a brief idea of various attempts made to improve the key factors affecting the overall performance of TiO₂ nanowire based DSSCs. From the large collection of literature on TiO₂ nanowire based DSSCs, here we are selectively discussing major research outcomes involving efficient synthesis methods for nanowires, novel architectures and significantly enhanced efficiencies. Many of the nanowire synthesis methods were based on hydrothermal treatment with slight modifications.

Feng et al. presented a straightforward low-temperature method to fabricate single-crystalline rutile TiO2 nanowires through a nonpolar solvent/hydrophilic solid substrate interfacial reaction under hydrothermal conditions. 75 Nanowires having lengths up to 5 µm can be grown vertically from the TCO glass substrate along the preferred direction by this approach. This arrangement has given an efficiency of 5.02% under AM1.5 irradiation by employing N719 dye on 2–3 μm long TiO₂ nanowire arrays. An added advantage of this technique is the low temperature employed, which favours the use of polymers for cell fabrication. Thus, low-temperature methods of photoanode fabrication are found to be compatible with polymer substrates and can result in flexibility. As part of developing flexible and lightweight DSSCs, Liao et al. introduced hierarchial TiO2 nanowire (HNW) arrays grown on a Ti foil substrate instead of FTO.125 These HNW arrays contain long TiO2 nanowire trunks and short TiO2 nanorod branches and are prepared by a twostep hydrothermal process. Liao et al. are the first to report such HNW arrays fabricated on Ti foil and they also replaced the Pt counter electrode with another electrode in which PEDOT is electrodeposited on the ITO-PET substrate. Even though HNW array DSSCs showed increased efficiency (4.32%) compared to that of NW-based DSSCs, the former possesses a comparatively reduced electron lifetime and transport time. As a further step toward realising lightweight and flexible DSSCs, cells were constructed with a vertical TiO2 nanowire array grown in situ on carbon fibre substrates as shown in Fig. 7.126



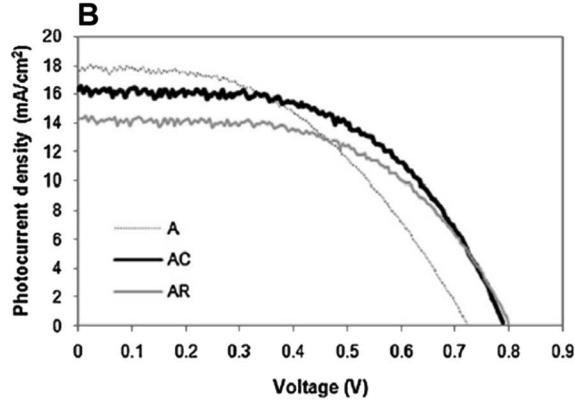


Fig. 8 (a) FE-SEM image of the cross sectional view of a double-layer film containing TiO_2 nanoparticles as the under-layer and corn-like TiO_2 nanowires as the over-layer. (b) Photocurrent density-voltage curves of fabricated TiO_2 solar cells [A- TiO_2 NP solar cell, AC- Corn like TiO_2 NW solar cell, AR-Regular TiO_2 NW solar cell]. (Reprinted with permission from ref. Bakhshayesh, A. et al., 2013. Copyright 2012 Elsevier Ltd.)

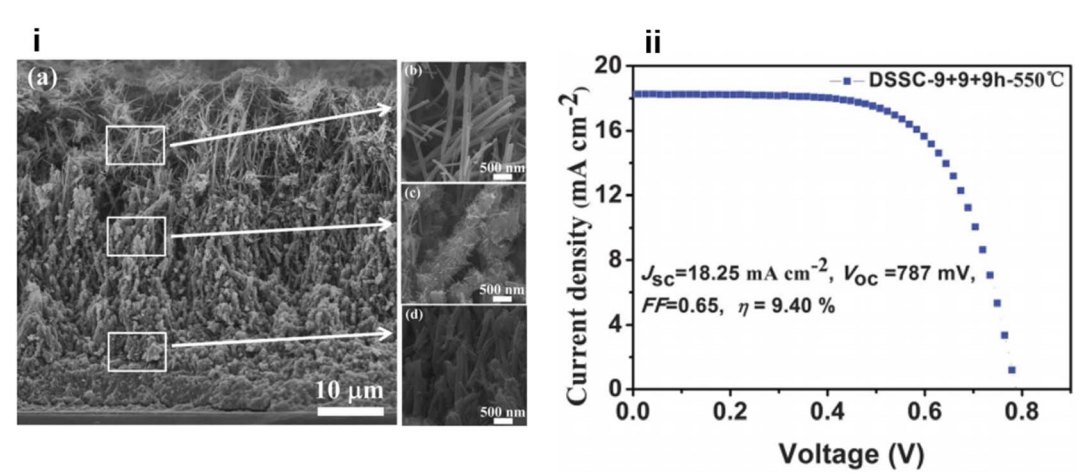


Fig. 9 (i) (a) The cross-sectional SEM images of MTNWs on FTO glass prepared after three hydrothermal cycles (9 + 9 + 9 h); (b, c, and d) the FESEM images of the upper, intermediate and bottom layers of the as prepared MTNWs, respectively. (ii) J-V characteristic of DSSCs based on the 47 mm thick TiO₂ NWs prepared with 3 hydrothermal cycles and followed by 550 °C calcination treatment.¹³⁴ (Reprinted with permission from ref. Wu *et al.*, 2014. Copyright 2013 Royal Society of Chemistry.)

In 2015, Liu et al. reported the controllable formation of TiO₂ nanowire arrays on a titanium mesh. This method is a hydrothermal one capable of forming nanowire arrays (NWAs) with an average diameter of 80 nm.127 Along with studying the influence of NWA preparation conditions on DSSC parameters, Liu et al. also focused on the role of the sensitization temperature and time on DSSC performance.127 They found that a higher sensitization temperature would benefit dye molecule infiltration to the internal areas of NWA films, and the complete covering of monolayer dye molecules on the surface of TiO2 NWAs would enhance the photovoltaic properties of the DSSC. By maintaining optimum conditions, Liu et al. obtained an efficiency of 3.42% for a flexible DSSC. Apart from maintaining optimum dye pickup, they were found to have depressed charge recombination also. Later several groups tried enhancing the available surface area of the photoanode by growing additional structures on TiO2 nanowires. In 2014, single-crystal-like 3D TiO₂ branched nanowire arrays were fabricated by Sheng et al. with the 1D branch epitaxially grown from the primary trunk. 128 This attempt made by Sheng et al. increased the available surface area by 71% and they also exhibited a fast charge transport property compared to one-dimensional TiO₂ nanowires. Sheng obtained an efficiency of 4.61% for branched nanowire-based DSSCs. 128 It is found that the presence of other nanostructures as branches on nanowires creates additional boundaries in electron transport. Later, DSSCs with multilayered photoanodes, in which different functions were assigned to specific layers, were fabricated. For example, in 2013, Bakshayesh et al. introduced a new TiO2 structure with corn-like nanowire morphology having high surface area and crystallinity synthesised by the surface tension stress mechanism. 129 They have adopted a double-layer DSSC design consisting of an underlayer of anatase TiO2 nanoparticles and an overlayer of corn-like TiO₂ nanowires as shown in Fig. 8a and Fig. 8b shows the photocurrent against voltage curves. By adopting a triple function mechanism with effective management of light

scattering, dye sensitization and photogeneration of charge carriers, Bakshayesh et al. attained an efficiency of 7.11%. Here the increased surface area of corn-like nanowires resulted in improved dye sensitization and short circuit current density. At the same time, the presence of NPs on corn-like nanowires increased light scattering. Most of the multilayer photoanodes follow such division of labour among various layers. Another new morphology reported in 2013 consists of thornbush like TiO₂ nanowires (TBWs) prepared by a facile single-step hydrothermal method using potassium titanium oxide oxalate dehydrate, diethylene glycol (DEG) and water at 200 °C.130 These TBWs consist of a large number of nanoplates and nanorods. Depending on the change in the DEG/water composition, the diameter, as well as the morphology of TBWs, varies. TBWs having a diameter of 200 nm shows higher efficiency (5.2%) than those having a diameter of 400 nm (4.5%) and 600 nm (3.4%). Further treatment of TBW200 with graft-copolymerdirected, organized mesoporous TiO2 helps to increase the surface area and interconnectivity of TBWs leading to an enhanced efficiency of 6.7%. As the electron transport in TiO₂ nanowires depends on their length, efforts were made to modify the nanowire length. In 2011, a multicycle hydrothermal synthetic process to produce vertically oriented, single-crystalline rutile TiO₂ nanowires with lengths in between 1 and 8 µm was reported by Zhou and co-workers.131 It is observed that a further increase in the nanowire length does not give an expected increase in efficiency. This can be attributed to a decrease in surface area by fusion and widening at the base of nanowires.

In the same year, a double-sided brush-shaped (DSBS) TiO₂ nano architecture consisting of highly ordered TiO₂ nanowires aligned around an annealed TiO₂ nanoparticle layer was prepared by C. Zha and team *via* the hydrothermal method. Here nanowire growth is seeded by the annealed nanoparticle layer and it supports the DSBS structure. It was found that by varying the hydrothermal reaction time, structural properties

This article is licensed under a Creative Commons Attribution 3.0 Unported Licence. Open Access Article. Published on 30 akamánnu 2022. Downloaded on 2025-11-01 08:56:03.

Table 1 TiO₂ nanowire-based DSSCs

DSSC Type	Author	Photoelectrode and method of preparation	Sensitizer	Electrolyte	Efficiency	Ref.
DSSC with ${\rm TiO_2}$ nanowire arrays	Feng <i>et al.</i>	Vertically aligned single-crystalline TiO ₂ nanowire arrays by nonpolar solvent/hydrophilic solid substrate interfacial reaction under hydrothermal conditions	N719	MPN-100 (Solaronix, Inc., Switzerland) containing tri-iodide in methoxypropionitrile	5.02%	75
DSSC with hierarchical TiO ₂ nanowires (HNW)	Liao <i>et al.</i>	Hierarchical TiO ₂ nanowire (HNW) arrays grown on a Ti foil substrate instead of FTO by a two step hydrothermal process	N719	I ⁻ /I ₃ ⁻ based liquid electrolyte, which contained 1-methyl-3-propylimidazolium iodide (PMII), guanidiium thiocyanate and <i>tert</i> -butylpyridine in acetonitrile and valeronitrile	4.32%	125
DSSC with a TiO ₂ nanowire array grown <i>in situ</i> on carbon fibre	Cai et al.	Vertically aligned TNW arrays <i>in situ</i> grown on carbon fiber (CF) substrates through a facile, controllable, and seed-assisted thermal process.	N719	12, 1,3-dimethylimidazolium iodide, 4-tert- butylpyridine, guanidine thiocyanate, and TiClO. in acetonitrile	4.18%	126
DSSC with TiO ₂ nanowire arrays on a titanium mesh	Liu et al.	Controllable formation of TiO ₂ nanowire arrays with average diameter 80 nm on a titanium mesh by a hydrothermal method	N719	12, 13-dimethylimidazolium iodide, 4-tert- 12, 13-dimethylimidazolium iodide, 4-tert- 12,00-in acetonitrile	3.42%	127
DSSC with 3D ${ m TiO_2}$ branched nanowire arrays	Sheng <i>et al.</i>	Single-crystal-like 3D TiO ₂ branched nanowire arrays consisting of a 1D branch epitaxially grown from the primary trunk prepared by a solvothermal method followed by exposure to O ₂ plasma	N719	1-Hexyl-2,3-dimethylimidazolium iodide and iodine in methoxypropionitrile	4.61%	128
DSSC with TiO ₂ nanowires and TiO ₂ NPs	Bakshayesh <i>et al.</i>	Double layered photoanode having corn like TiO ₂ nanowires prepared by a surface tension stress mechanism	N719	Dimethylpropylimidazolium iodide, LiI, I ₂ , and 4-tert-butylpyridine in acetonitrile	7.11%	129
DSSC with thornbush like	Roh et al.	Thornburning The TiO ₂ nanowires (TBWs) prepared by a facile single step hydrothermal method	N719	Dimethylpropylimidazolium iodide, Lif, I ₂ , and 4-fort-burk-lawridine in acetonitrile	6.7%	130
DSSC with TiO_2 nanowire array films	Zhou et al.	Vertically oriented, single crystalline rutile TiO ₂ nanowires by a multicycle hydrothermal synthetic	N719	Lif. 12, 1,2-dimethyl-3-n-propylimidazolium iodide (DMPII), and tert-butylpyridine in debudrated aceronitrile	2.0%	131
DSSC with TiO ₂ nanowires and TiO ₂ NPs	Zha <i>et al.</i>	process Double sided brush shaped (DSBS) TiO ₂ nano architecture consisting of highly ordered TiO ₂ nanowires aligned around an annealed TiO ₂ manoparticle layer was prepared by a hydrothermal	N719	1-Butyl-3-methyl imidazolium iodide, I ₂ , guanidinium thiocyanate, and 4-tert- butylpyridine in a mixture of acetonitrile and valeronitrile	5.61%	132
DSSC with TiO ₂ nanowire	Wu et al.	Vertically aligned anatase TiO ₂ nanowires on FTO glass with a tunable length in the range of 15–55 mm for multilayered configuration of the photoanode by a hydrothermal method	N719	Γ/I_3^- redox electrolyte	9.40%	134
DSSC with multistacked three dimensional, hyperbranched titania	Wu et al.	Photoelectrode with multistacked layers having integrated functions	N719	1-Methyl-3-propylimidazolium iodide (PMII), LiI guanidinium thiocyanate, I ₂ , and <i>tert</i> - butylpyridine in acetonitrile and valeronitrile	11.01%	135
DSSC with TiO ₂ nanowires	Jiang <i>et al.</i>	TiO ₂ nanowire array electrodes are prepared by a hydrothermal method followed by silanization	N719	Ferrocene (Fc), ferrocenium tetrafluoroborate (Fc ⁺), and tetrabutylammonium tetrafluoroborate	0.749%	146
DSSC with TiO ₂ nanowires	Li, H. <i>et al.</i>	Vertically aligned rutile ${\rm TiO_2}$ nanowire arrays (NWAs) by a single step solvothermal method without using any surfactant or template	C106	DMII, LiI, I ₂ , TBP, and GNCS in the mixture of acetonitrile and valeronitrile	8.9%	136

_
7
Chr
Ç
_
7
Tak
•

DSSC Type	Author	Photoelectrode and method of preparation	Sensitizer	Electrolyte	Efficiency	Ref.
DSSC with a TNW-AuNP hybrid structure	Yen et al.	3D TNW-AuNP plasmonic electrode prepared by hydrothermal and sputtering techniques	N719	I ₂ , LiI, DMPII, and TBP in acetonitrile	9.73%	137
DSSC with NP/NW composite films	Lee et al.	TiO ₂ nanoparticle (NP)/nanowire (NW) composite films with various compositions are prepared by a solvothermal method	MK-2 dye	Cobalt redox couple	7.37%	138
DSSC with a TiO ₂ nanowire network	Jin et al.	TiO ₂ nanowire networks on Ti foil using a Ti corrosion reaction	N719	Iodolyte AN-50, Solaronix, Aubonne, Switzerland	1.11%	139
DSSC with TiO ₂ nanowire networks	Shin et al.	TiO ₂ nanowire networks on FTO substrates by wet corrosion	N719	Iodolyte AN-50, Solaronix	1.0%	140
DSSC with TiO ₂ nanowires	Li et al.	Single crystalline self-branched anatase TiO ₂ NWs by a hydrothermal method using TBAH and CTAB as co-surfactants	N719	Lif, I ₂ , dimethylpropylimidazolium iodide (DMPImI) and <i>tert</i> -butylpyridine in a dry mixed solution	6.37%	141
DSSC with a ${ m Ti}@{ m Ti}{ m O}_2$ nanowire array	Liu <i>et al.</i>	Spring like Ti@TiO ₂ nanowire array was prepared by a hydrothermal technique at a controlled NaOH concentration	N719	1,3-Dimethylimidazolium iodide I., LiClO ₄ , 4- tert-butylpyridine and guanidine thiocyanate in acetonitrile	2.787%	142
DSSC with a rutile TiO ₂ nanowire array	Ni et al.	Rough surface rutile TiO ₂ nanowire array prepared by a hydrothermal method and prolonged etching. An additional light scattering layer of TiO ₂ particles was also employed	C109	1,3-Dimethylimidazolium, lithium iodide, iodine, <i>tert</i> -butylpyridine, and guanidinium thiocyanate in acetonitrile and valeronitrile	9.39%	143
DSSC with reduced graphene encapsulated TiO ₂ -B nanowire composite	Makal <i>et al.</i>	Reduced graphene oxide encapsulated TiO ₂ –B nanowire composite synthesized by a hydrothermal method	N3	Iodolyte AN-50	4.95%	144
DSSC with a g-C ₃ N ₄ encapsulated TiO ₂ -B nanowire composite	Makal <i>et al.</i>	g-C ₃ N ₄ encapsulated TiO ₂ -B nanowire composite synthesized by thermal calcination of hydrothermally grown TiO ₂ -B nanowires and melamine	N3	Iodolyte AN-50	5.12%	145

like the crystalline phase, phase composition, length of the nanowires and thickness of the nanoparticle layer can be tuned. They have obtained an efficiency of 5.61% from an 8 hour reaction time and nanowires of length 6 µm. Thus, the microstructure has a significant influence on solar cell performance and the DSBS structure is a greatly promising one. Later Qiang Wu and co-workers fabricated a DSSC based on a self-assembled, vertically aligned TiO₂ nanowire photoelectrode sensitized with N719 (ref. 133) sensitizer and it could achieve an efficiency of 9.40% (Fig. 9).134 Here TiO2 nanowires on an FTO glass plate have a tuneable length in the range of 15-55 µm and are suitable for multi-layered photoanode configuration.¹³⁴ The same team of Wu et al. reported another distinct and novel architecture with the integration of various three-dimensional, hyperbranched titania nanoarchitectures into a multi-stack. The multi-stacked layers consist of an underlayer of hyperbranched hierarchical tree-like titania nanowires, branched hierarchical rambutan-like titania hollow submicrometer-sized spheres as the intermediate layer and hyperbranched hierarchical urchin-like titania micrometre-sized spheres as the top layer.135 Here the bottom layer enhances electron transport through one-dimensional nanowires into the FTO plate whereas the middle layer can guarantee effective light-trapping efficiency through the hollow-hole structure of submicrometersized macroporous TiO₂ spheres and the upper layer of hyperbranched hierarchical TiO₂ microspheres can offer increased light scattering ability. This integrated photoanode achieved an

efficiency of 11.01% which is far better compared to that of its TiO2 NP analogue.

In 2016, Hailiang Li et al. constructed vertically aligned rutile TiO₂ nanowire arrays (NWAs) with a length of ~44 μm on transparent conductive fluorine-doped tin oxide (FTO) glass by a facile one-step solvothermal method without using any surfactant or template. 136 By controlling the ethanol content in the reaction mixture, the length and separation between the NWs can be controlled. A reaction mixture containing 20 mL ethanol facilitated the formation of TiO2 NWAs with an efficiency of 8.9%. This can be further enhanced to 9.6-10.2% by incorporating a light scattering layer into the TiO2 NWA-based DSSC.

Another mode of enhancement of light absorption and efficiency of DSSCs utilizes the anti-reflecting (AR) property of photoanode materials. Another approach is by the exploitation of the surface plasmonic effect of metal nanoparticles. Yen et al. fabricated a DSSC utilizing both the antireflecting character and plasmonic effect. Their DSSC was equipped with a 3D TNW-AuNP plasmonic electrode having antireflective (AR) TiO2 nanowires (TNWs) serving as light-harvesting antennae coupled with Au nanoparticles (NPs).137 These plasmonic functionalized electrodes (PFEs) exhibited a remarkable plasmonic red shift from 520 nm to 575 nm. Such PFEs were developed to overcome the narrow absorption range and low absorption coefficient of dyes. It was found that TiCl4 treatment can increase the efficiency of TNW-AuNP hybrid DSSCs from 6.25% to 9.73%. In the same year, Lee et al. investigated the photovoltaic performances

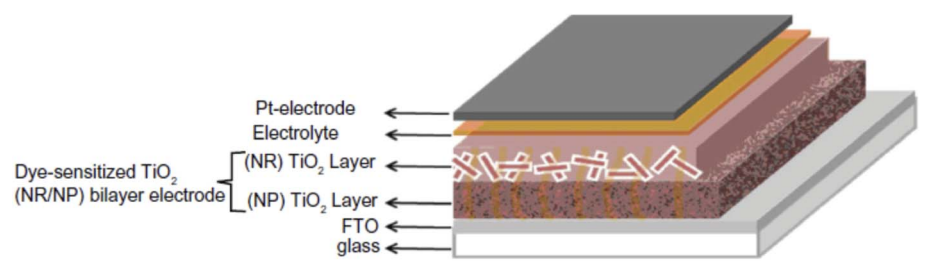


Fig. 10 Schematic representation of the DSSC based on a TiO₂ NR/NP bilayer photoanode.¹⁵⁰ (Reprinted with permission from ref. Hafez et al., 2010. Copyright 2010 Hafez et al., publisher and licensee Dove Medical Press Ltd.)

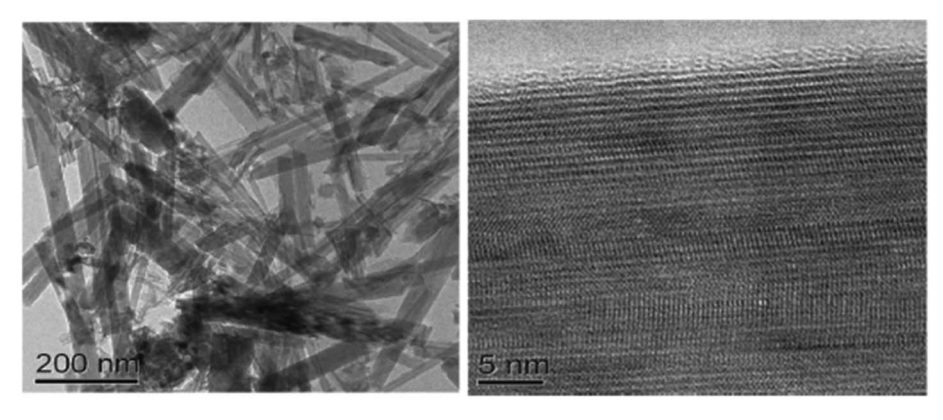
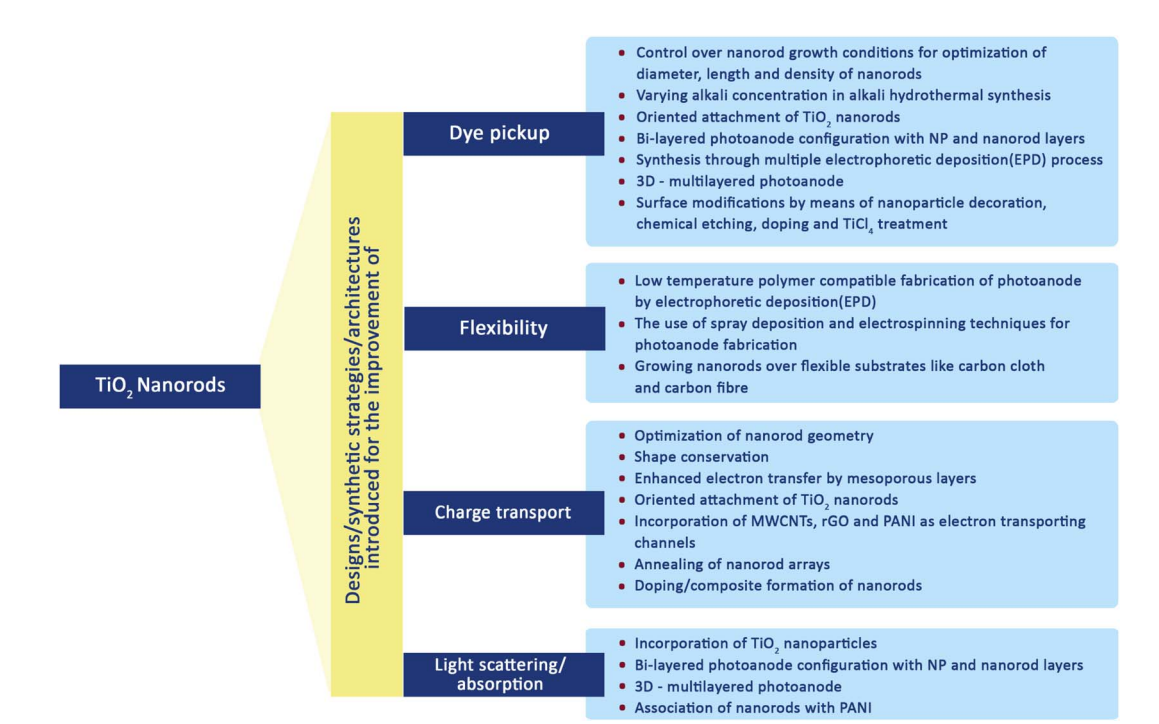


Fig. 11 TEM images of the TiO₂ nanorod sample and the HRTEM image of the nanorod. 150 (Reprinted with permission from ref. Hafez et al., 2010. Copyright 2010 Hafez et al., publisher and licensee Dove Medical Press Ltd.)



Scheme 2 Various modifications introduced for the improvement of the performance of TiO₂ nanorod based DSSCs.

of back-illuminated DSSCs employing TiO2 NP/NW composite films of various weight percentages. 138 These DSSCs used a cobalt-based electrolyte system. In NP/NW composite films NPs help to increase the surface area whereas NWs facilitate efficient charge transfer. The highest efficiency of 7.37% was shown by DSSCs with 10 wt% of NWs in the NP/NW composite film which is 20% improved compared to that of a pure NPbased DSSC. Apart from the widely used hydrothermal method of nanowire synthesis, Jin et al. proposed an approach for fabricating TiO2 nanowire networks on Ti foil using a Ti corrosion reaction in KOH aqueous solutions at different temperatures, followed by a further ion-exchange process. 139 These photoanodes were suitable for bendable DSSCs and have exhibited an efficiency of 1.11% for back illumination. The same team also tried growing TiO2 nanowire networks on FTO substrates by wet corrosion and obtained an efficiency of 1.0% under AM 1.5 illumination. 140 In 2017 Li and co-workers reported a simple single-step hydrothermal method to prepare single-crystalline self-branched anatase TiO2 NWs by using TBAH and CTAB as co-surfactants.141 These single crystalline self-branched TiO2 NW-based DSSCs exhibited an efficiency of 6.37% which is due to an enhanced percentage of exposed (010) facets having high dye adsorption capacity. Again in 2018, another design was introduced into the class of FDSSCs (fiber shaped dye-sensitized solar cells) which consists of a stretchable spring-like Ti@TiO₂ nanowire array as the photoanode by Liu and co-workers. This design was intended to achieve higher flexibility and elasticity of DSSCs and the spring-like Ti@TiO2 array was prepared by the hydrothermal technique at a controlled NaOH concentration. Liu's team was the first to achieve a 100% stretching degree in FDSSCs with a PCE

retention rate of 95.95% upon bending accompanied by 100% stretching strain.142 Another major finding was made by Ni et al., that the enhanced surface area of nanowire arrays achieved on prolonged etching treatment can improve the dye intake but it reduces the PCE by increased electron recombination. Even then, Ni and co-workers succeeded in attaining an improved PCE of 9.39% by employing an additional scattering layer of TiO2 particles along with rough surface rutile TiO2 nanowire arrays.143 Thus, light scattering layers can make up for the loss encountered by extended rates of photo electron recombination. As a way of minimising charge recombination and improving electron transport across TiO₂ nanowires, developing composites with materials having high electrical conductivity and charge carrier mobility was found exciting. One such approach was carried out by Makal and Das in 2021 by fabricating a reduced graphene oxide laminated one-dimensional TiO2-B nanowire composite based photoanode. 144 The effect of different reduced graphene oxide loadings on the PCE of the DSSCs was evaluated and it was found that an 8 wt% loading showed a PCE of 4.95%. Makal and Das used the same design to develop another photoanode material where they encapsulated TiO2-B nanowires with graphitic carbon nitride (g-C₃N₄) and the PCE for the developed cell was found to be 5.12%. This is one of the highest efficiencies reported for a DSSC with a TiO2-B based photoanode. Significant efforts carried out for increasing the performance of nanowire-based DSSCs are discussed above and are tabulated in Table 1.

3.2. Nanorods

Nanorods (NRs) are introduced into DSSC photoanode fabrication (Fig. 10) with the objective of increasing DSSC

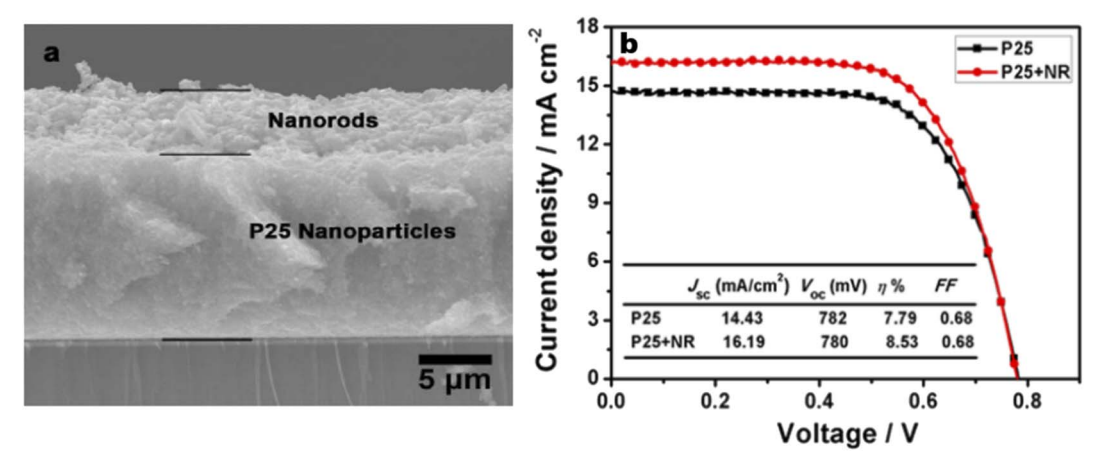


Fig. 12 (a) Cross section SEM image of the bi-layer structured photoanode with a P25 nanoparticle bottom layer and porous nanorod top layer; (b) comparison between J-V curves of cells based on the bi-layer photoanode and single-layer P25 photoanode with the same thickness. Reprinted with permission from ref. Chen, H.-Y. et al., 2013. Copyright 2013 American Chemical Society.)

performance by exploiting their one-dimensional nanoscale properties. ${\rm TiO_2}$ nanorods facilitate easy electron transfer by utilising their specific geometry (Fig. 11) and reducing the ohmic loss during the electron transfer through the mesoporous titania layer. 147 Various methods have been used for the synthesis of ${\rm TiO_2}$ nanorods for DSSC applications. Along with the introduction of novel synthesis strategies, efforts were made to modify the morphology and surface properties of ${\rm TiO_2}$ nanorods as given in Scheme 2.

A widely used fabrication method for TiO2 nanorods was the solvothermal method. Several studies on TiO2 nanorods were reported based on solvothermal techniques. 147-160 Most of the solvothermal methods used for TiO2 nanorod fabrication employ water as a solvent i.e. the hydrothermal method. Sometimes the solvothermal method may be a multi-step process or a combination of more than one synthetic method. In 2005 Jiu et al. reported the synthesis of single crystalline anatase TiO2 nanorods by a surfactant-assisted hydrothermal method. These nanorods were found to exhibit an efficiency of 7.06%. Higher fill factor (FF) values of TiO₂ NRs were observed compared to those of P25 nanoparticles, indicating the easier electron transport (lower resistance) through nanorods. In 2006, Jiu et. al. prepared single-crystalline anatase TiO2 nanorods by a surfactant-assisted hydrothermal method with control over the size and diameter. Here nanorods having a length of 100-300 nm and diameter of 20-30 nm were synthesized and they showed an efficiency of 7.29%.147 Jiu et al. achieved shape conservation and size regulation of nanorods with the help of a copolymer. Later Liu et al. found that the diameter, length and density of the nanorods prepared by the solvothermal method could be varied by changing the growth conditions such as growth time, growth temperature, initial reactant concentration, acidity and additives.161 Efforts of Liu et al. resulted in the formation of single-crystalline rutile TiO2 nanorods having an efficiency of 3%. In the very next year, a significant increase in conversion efficiency (7.9%) was achieved by De Marco et al. using TiO2 nanorods prepared by a single-step solvothermal

technique.149 The obtained anatase TiO2 nanorod crystals were converted into screen printable paste for easy application into DSSCs. Here the solvothermal method helped to avoid coarse aggregation and shape loss of nanorods. Using the alkali hydrothermal technique, a novel morphology i.e. fan-shaped rectangular parallelepiped TiO2 rods were synthesized by Shao et al. with a conversion efficiency of 6% obtained for 1 M NaOH utilizing DSSCs and this efficiency is found to be 66.7% higher than that of P25-DSSCs. 153,162 Investigations carried out at different NaOH concentrations showed that the morphology and crystal phase of the nanorods are affected by the alkali concentration. Kathirvel et al., Liu et al. and Zhang et al. reported the highest efficiencies for solvothermal derived TiO₂ nanorods. 158-160 Oriented rutile TiO2 nanorod arrays were grown in situ on an FTO (fluorine doped tin oxide) coated glass substrate by using a mixed acid medium composed of titanium tetraisopropoxide (TTIP), hydrochloric acid (HCl), acetic acid (AcOH) and water (H2O) as the solvent. 152 An acid mixture with HCl: AcOH in a volume ratio of 4:8 produced oriented, uniform, thin rutile nanorods which were found to be superior to single acid-grown nanorods. They have shown an efficiency of 4.03% using 2.3 µm long nanorods. Zhang and co-workers introduced an oriented attachment mechanism for the fabrication of size and shape tuneable anatase TiO2 NRs. 158 These single crystalline long TiO2 NRs have reduced grain boundaries which lead to enhanced charge collection. Thus, long thin NRbased DSSCs exhibited an efficiency of 8.87%. In 2015 Liu et al. prepared single-crystalline anatase TiO2 nanorods by a solvothermal method in which tetrabutylammonium hydroxide (TBAH) is used as the morphology controlling agent. 159 DSSCs fabricated using these NRs have achieved an efficiency of 8.66%. Recently, several single and multi-step solvothermal fabrications of TiO2 NRs were reported. 160,163-165 Later it is found that employing a composite structure of nanorods (NR) and nanoparticles (NP) in the photoanode can complement the advantages of each other. The first bilayer NR/NP composite structured photoanode was fabricated by Hafez et al. 150 Here the

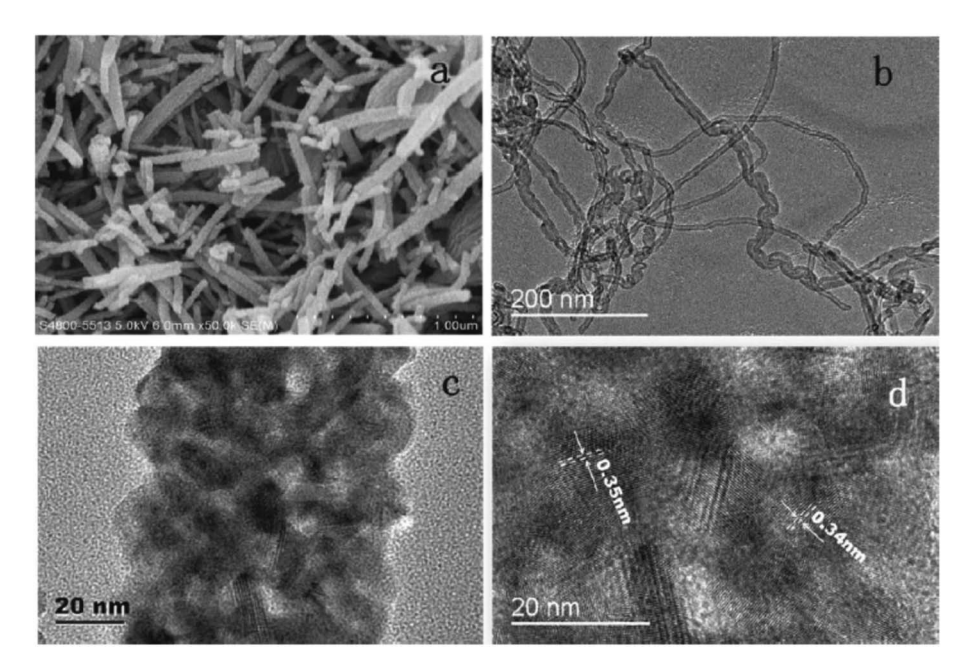


Fig. 13 SEM and TEM images: (a) SEM image of TiO_2 nanorods incorporating MWCNTs; (b) and (c) are TEM images, respectively, of MWCNTs and TiO_2 nanorods incorporating MWCNTs; (d) HRTEM image of TiO_2 nanorods that incorporate MWCNTs.¹⁷⁵ (Reprinted with permission from ref. Yang and Leung, 2013.Copyright 2013 WILEY-VCH Verlag GmbH & Co. KGaA, Weinheim.)

sol-gel derived NP layer was coated with hydrothermally prepared NRs and this DSSC assembly exhibited an efficiency of 7.1%. Several NR/NP bilayered photoanode structures were fabricated later. 151,155,156,166-170 These bilayer structures provided enhanced light scattering as well as increased surface area, which is finally reflected in their increased efficiencies (Fig. 12). The bilayer design proposed by Rui and co-workers enabled the synthesis of size tuneable rutile TiO2 nanorod microspheres by controlled hydrolysis during solvothermal synthesis and can be employed as a scattering over-layer in bilayer DSSCs. 156 Rui et al. achieved an efficiency of 8.22% whereas the efficiency of the single layer reference cell was 7.00%. Better performance of the TiO2 NP/NR composite was obtained by Chatterjee and coworkers by employing a 1:1 wt% composite obtained from hydrothermally derived NRs and commercially available TiO2 powder.171 The obtained PCE of 8.61% was the highest among the photoanodes fabricated out of TiO2 NR/NP composites. Shao et al. introduced low-temperature fabrication of photoanodes for flexible DSSCs by electrophoretic deposition (EPD).167 The obtained NR/NP structures (NRPs) have high surface charges and wide size distribution. In addition, a multiple EPD process was adopted to form a better quality microstructured photoanode. In the same total time, the efficiencies of the multiple devices are more than 2.2 times that of one-step devices. Without any calcination or compression, the best device fabricated with multiple EPD and a thin layer of nanoparticles gives a conversion efficiency of 4.35%. Using a two-step hydrothermal method a novel bilayer structure composed of one-dimensional nanorods, which can serve as direct electron transport pathways and a three-dimensional hierarchical structure acting as a light scattering as well as large surface area layer for dye loading was introduced by Li et al. 168

The dependence of the TiO2 NR/NP structured composite's photoanode efficiency on the amount of NRs was studied by researchers and it was found that efficiency is the maximum for composites having 10% NR content (4.89%). Another method employed for nanorod synthesis was electrospinning. Fujihara et al. employed electrospun TiO2 nanofibres as precursors for nanorods and these rods were spray dried onto an FTO plate. 173 These spray deposited nanorods overcame the adhesion difficulties of nanofibres and exhibited an efficiency of 5.8%. Another electrospun synthesis was done by Jose et al. and they yielded 5.1% efficiency. 190 In 2009 DSSCs having an efficiency of 9.52% were fabricated by Lee et al. using a combination of solgel and electrospinning techniques. Here nanorods were electrospun from a solution of titanium n-propoxide and polyvinyl acetate in dimethyl formamide.174 They have conducted a comparative study of nanorod and nanoparticle based DSSCs. These studies revealed that nanorod DSSCs have a pore volume double that of nanoparticle cells. Obviously the surface area available for sensitizers in nanorods is ~2.5 times that of the nanoparticle based DSSC at equal TiO2 weights. Also, the electron-hole recombination time for nanorods is found to be more than eight times that of nanoparticle DSSCs. Later in 2013 MWCNTs were introduced as electron transporting superhighways into TiO2 nanorods by the electrospinning technique (Fig. 13). This incorporation was done by Yang et al. and they obtained an efficiency of 10.24%. 175 In the same year Chen et al. employed a microemulsion electrospinning technique to synthesize TiO2 nanorods as a composite of mesopores and macropores by using paraffin oil droplets as the template.166 This microemulsion electrospinning approach achieved 8.53% efficiency for bilayer DSSC architecture with NRs as the scattering layer.

Table 2 TiO₂ nanorod-based DSSCs

1						
DSSC Type	Author	Photoelectrode and method of preparation	Sensitizer	Electrolyte	Efficiency	Ref.
DSSC with TiO ₂ nanorods	Jiu <i>et al.</i>	TiO ₂ single crystalline anatase nanorods prepared by a surfactant assisted hydrothermal method	N719	Lif, 1,2-dimethyl-3- <i>n</i> -propylimidazolium iodide (DMPII), I ₂ , and 4- <i>tert</i> -butylpyridine (TBP) in	7.06%	148
DSSC with TiO ₂ nanorods	Jiu <i>et al.</i>	Highly crystalline TiO ₂ nanorods synthesized by a hydrothermal process in a cetyltrimethylammonium bromide	N719	methoxyaccondinate Lil, 1,2-dimethyl-3-n-propylimidazolium iodide (DMPII), 12, and 4-tert- burklpyridine (TBP) in	7.29%	147
DSSC with TiO ₂ nanorods	Yao et al.	Surfactant Solution Monodispersed Nd-doped ${\rm TiO_2}$ nanorods were synthesized by solvothermal methods	N719	Lil, I ₂ , and 4-tert-butylpyridine in 3-methoxypropionitrile	4.4%	183
DSSC with TiO ₂ nanorods	Fujihara <i>et al.</i>	TiO ₂ nanorods were obtained by mechanical grinding of electrospun TiO ₂ nanofibers	N3 Solaronix	Acetonitrile containing lithium iodide, iodine, <i>4-tert</i> -butylpyridine and 1-propyl-2-3-dimerkyi imidazolium iodide	5.8%	173
DSSC with TiO ₂ nanorods	Jose et al.	${ m TiO_2}$ nanorods by electrospinning	D131, D102, D149 & N3	Action of the state of the stat	5.1%	190
DSSC with TiO ₂ nanorods	Kang <i>et al.</i>	${\rm TiO_2}$ nanorods prepared by an oriented attachment approach	N719	1. Methyl-3-propylimidazolium iodide (MPII), LiI, 1 ₂ , and <i>tert</i> -butyl pyridine (TBP) in methoxoniconionitrile (MPN)	6.2%	191
DSSC with ${ m TiO_2}$ nanorods	Lee <i>et al.</i>	TiO ₂ nanorod based photoelectrodes prepared by a combination of sol–gel chemistry and electrospinning	N719	1-Buylan meansy proposition (2017) 1-Buylan-ethylimidazolium iodide, iodine, guanidinium thiocyanate, and 4- tert-buylpyridine in acetonitrile/ valeronitrile	9.52%	174
DSSC with ${ m TiO_2}$ nanorods	Liu <i>et al.</i>	Oriented single-crystalline rutile TiO ₂ nanorod films prepared by a hydrothermal method	N719	tarconnence the state of the st	3.0%	161
DSSC with ${\rm TiO}_2$ nanorods	De Marco <i>et al.</i>	TiO_2 anatase nanorods prepared by a simple one-step solvothermal method	N719	Lil, I ₂ , 1-methyl-3-propylimidazolium iodide, and <i>tert</i> -butylpyridine in dried	7.9%	149
DSSC with TiO ₂ nanorods	Hafez <i>et al.</i>	TiO ₂ nanorod/nanoparticle (NR/NP) bilayer electrode prepared by a hydrothermal method	N719	Tetrapropylammonium iodide, iodine, lithium iodide, and 4-tert-butylpyridine in acetonitrile	7.1%	150
DSSC with a TiO_2 NP/	Saji <i>et al.</i>	$_{\rm rio_2}$ NPs and NRs were prepared by a surfactant-assisted thermal method	N3	Lil, I ₂ , and <i>tert</i> -butyl pyridine in 3- methoxy propionitrile	4.89%	172
DSSC with TiO ₂ NRs/ NPs	Fan <i>et al.</i>	Anatase TiO ₂ fusiform nanorod/NP photoanode prepared by a two step hydrothermal process	N719	Lil, I ₂ and 4-tert-butylpyridine in 1 : 1 actonitrile propylene carbonate	4.68%	151
DSSC with TiO ₂ NRs/ NPs	Huang et al.	Ruffle TiO ₂ nanorod-array films grown from a mixed acid medium by a hydrothermal reaction	(2-Cyano-3-{5'-[1-cyano-2- (1,1,6,6-tetramethyl-10-oxo- 2,3,5,6-tetrahydro-1 <i>H</i> ,4 <i>H</i> ,10 <i>H</i> - 11-oxa-3 <i>a</i> -aza-benzo-[<i>de</i>] anthracen-9-yl)-vinyl]-[2,2] bithiophenyl-5-yl}-acrylic acid	Lil, I ₂ , DMPImI, and TBP using dehydrated AN as the solvent	4.03%	152

Open Access Article. Published on 30 akamánnu 2022. Downloaded on 2025-11-01 08:56:03.

BY This article is licensed under a Creative Commons Attribution 3.0 Unported Licence.

_	_	
1	_	
7	ì	
i	ć	
(_	j
`		
c	`	J
	0	J
	C	į
Ŀ	α	3

DSSC Type	Author	Photoelectrode and method of preparation	Sensitizer	Electrolyte	Efficiency	Ref.
DSSC with TiO ₂ NRs/ NPs	Chatterjee <i>et al.</i>	1:1 TiO ₂ NR-NP composites prepared by a hydrothermal technique with	N719	LiI, $\mathbf{I_2}$ and 4-t-butylpyridine in acetonitrile	8.61%	171
DSSC with TiO ₂ nanorod arrays	Shao <i>et al.</i>	Fan-shaped rectangular parallelepiped TiO ₂ rods were prepared by an alkali hydrothermal method	N719	Lil, 1 ₂ , and <i>tert</i> -butylpyridine in acetonitrile	%0.9	153
DSSC with branched rutile TiO ₂ nanorod arrays	Wang et al.	Rutile TiO ₂ nano-branched arrays grown directly on transparent conductive glass (FTO) by a facile two-step wet chemical synthesis process	N719	1,2-Dimethyl-3-propylimidazolium iodide, 1 ₂ , guanidinium thiocyanate, and 4-tert-butylpyridine	3.75%	176
DSSC with TiO ₂ nanorod arrays	Wang et al.	One dimensional ${\rm TiO}_2$ nanorod arrays prepared by a hydrothermal method	N719, C218 and D205	1-Propyl-3-methylimidiazolium iodide, I ₂ , guanidinium thiocyanate, NaI, and <i>N</i> -methyl benzimidazole in 3-methoxypropionitrile	1.51%(C218)	178
DSSC with ${ m TiO}_2$ nanorod cloths	Wang et al.	Single-crystal nanorod assembled TiO ₂ cloth with carbon cloth as a template were prepared by a rapid microwave heating process	N719	DMPII, Lil, I ₂ and 4-ТВР in methoxypropionitrile	2.21%	192
DSSC with ${\rm TiO}_2$ nanorods	Yang et al.	Single crystalline rutile nanorods grown on top of a fluorine doped tin oxide (FTO) substrate via a microwave assisted hydrothermal reaction	N719	Iodolyte AN-50, (Solaronix)	3.7%	193
DSSC with a Au NP deposited TiO ₂ nanorod array	Ghaffari <i>et al.</i>	Au nanoparticles were loaded onto the surface of hydrothermally prepared TiO_2 nanorods νia a photochemical reduction process	N719	Guanidinium thiocyanate (GuSCN), I ₂ , 4- tert-butylpyridine (TBP) and butylmethylimidazolium iodide (BMII) in a mixture of acetonitrile and valeronitrile	0.94%	181
DSSC with a ${ m TiO_2}$ nanorod array	Guo <i>et al.</i>	Rectangular bunched rutile TiO ₂ nanorod arrays grown on carbon fiber by an acid corrosion method	N719	Lif, 1 ₃ , and <i>4-tert</i> -butylpyridine in 3-methoxypropionitrile	1.28%	177
DSSC with ${ m TiO_2}$ nanorods	Liu et al.	Anatase TiO ₂ nanorods were prepared by a facile two-phase hydrothermal method	N719	Lif, 1 ₂ , 1-methyl- 3-propylimidazolium iodide, and <i>tert</i> -butylpyridine in dried acetonitrile	6.37%	154
DSSC with a spherical TiO ₂ nanorod-aggregate light-scattering layer	Liu et al.	Bilayer-structured photoelectrode film with spherical TiO ₂ nanorod aggregates as a light-scattering overlayer and nanocrystalline TiO ₂ as an underlayer prepared by a hydrothermal method	N719	Lil, I., 1,2-dimethyl-3-propylimidazolium iodide, and <i>4-tert</i> -butylpyridine in acetonitrile	6.1%	155
DSSC with TiO_2 nanorods having a composite structure	Chen <i>et al.</i>	Ultraporous anatase TiO ₂ nanorods fabricated by a simple microemulsion electrospinning approach	N719	I ₂ , LiI, 1-methyl-3-propylimidazolium iodide (PMII), guanidinium thiocyanate, and <i>tert</i> butylpyridine in a mixture of acetonitrile/valeronitrile	8.53%	166
DSSC with a spherical TiO ₂ nanorod-aggregate light-scattering layer	Rui et al.	TiO ₂ microspheres assembled by single crystalline rutile TiO ₂ nanorods were synthesized by one-pot solvothermal treatment	N719	I ₂ , LiI, 1-methyl-3-propylimidazolium iodide (PMII), guanidinium thiocyanate, and <i>tert</i> -butylpyridine in a mixture of acetonitrile/valeronitrile	8.22%	156

Open Access Article. Published on 30 akamánnu 2022. Downloaded on 2025-11-01 08:56:03.

| Prince | This article is licensed under a Creative Commons Attribution 3.0 Unported Licence.

7
÷
C
2
۰,
Ç
_
^
a
7
4
Table
Н

DSSC Type	Author	Photoelectrode and method of preparation	Sensitizer	Electrolyte	Efficiency	Ref.
DSSC with TiO ₂ nanorods and MWCNTs	Yang et al.	MWCNTs are introduced into TiO ₂ nanorods by electrospinning	N719	I ₂ , LiI, 1-methyl-3-propylimidazolium iodide (PMII) and 4- <i>tert</i> -butylpyridine in a mixture of acetonitrile/valeronitrile	10.24%	175
DSSC with a TiO ₂ nanorod based network structure	Yu et al.	Three dimensional rutile-nanorod-based network structure was developed by a facile two-step hydrothermal process	N719	Organic-based liquid electrolyte (HPE) that contained a Γ/I_3 redox couple was supplied by Dyesol (Australia)	6.31%	157
DSSC with a TiO ₂ nanorod/nanoparticle (NRP) structure	Shao et al.	NRP structured photoanodes prepared by electrophoretic deposition (EPD)	N719	Lif, I ₂ and <i>tert</i> -butylpyridine in acetonitrile	4.35%	167
DSSC with TiO ₂ nanorods	Zhang <i>et al.</i>	Single crystal-like anatase TiO ₂ nanorods with a specific growth direction are prepared by a hydrothermal method	Z907	$1,3$ -Dimethylimidazolium iodide, LiI, and I_2 in a mixture of acetonitrile and valeronitrile	8.87%	158
DSSC with a bilayered TiO ₂ photoanode	Li et al.	Bi-layer photoanode consisting of a hierarchical structure of one dimensional nanorods and three dimensional TiO ₂ was prepared by a hydrothermal method	N719	Lif, I ₂ , 1,2-dimethyl-3-propylimidazolium iodide (DMPII) and <i>4-tert</i> -butylpyridine (4-TBP)	5.61%	168
DSSC with ${ m TiO_2}$ nanorods	Liu et al.	Single-crystalline anatase TiO ₂ nanorods were prepared by a solvothermal method	N719	Lit, I ₂ , dimethylpropylimidazolium iodide (DMPImI) and <i>tert</i> -butylpyridine in dry acetonitrile	8.66%	159
DSSC with TiO ₂ nanorod arrays	Yuan <i>et al.</i>	Vertically ordered single-crystalline TiO ₂ nanorod arrays (NRAs) were prepared by a combination of hydrothermal and etching methods	N719	Lif, I ₂ , 1-propyl-3-methylimidazolium iodide and <i>tert</i> -butylpyridine in dry acetonitrile	4.69%	182
DSSC with ${ m TiO_2}$ nanorod arrays	Iraj <i>et al.</i>	Vertically aligned rutile TiO ₂ nanorod arrays were synthesized by a hydrothermal method	N719	Lif, I ₂ , 1-propyl-3-methylimidazolium iodide and <i>tert</i> -butylpyridine in dry acetonitrile	1.86%	165
DSSC with TiO ₂ nanorods	Kathirvel et al.	Monodispersed TiO ₂ nanorods were prepared using a simple solvothermal process	N719	Lithium iodide, iodine, <i>4-tert</i> -butylpyridine and 1,2-dimethyl-3-propylimidazolium iodide was dissolved in acetonitrile	9.21%	160
DSSC with ${ m TiO_2}$ nanorods	Tang et al.	Single-crystalline anatase TiO ₂ nanorods with a high aspect ratio	N719	Lit, I., dimethylpropylimidazolium iodide (DMPImI) and <i>tert</i> -butylpyridine in a dry mixed solution	7.51%	189
DSSC with TiO ₂ nanorods	Guli et al.	TiO ₂ nanorod arrays were synthesised through a facile one-step solvothermal route without any surfactant and template	N719		1.68%	163
DSSC with branched hierarchical TiO ₂ nanorod arrays	Hu et al.	Rutile branched hierarchical TiO ₂ nanorod arrays were prepared by a facile two-step hydrothermal method	N719	Lif, I ₂ , 1-propyl-3-methylimidazolium iodide and <i>tert</i> -butylpyridine in dry acetonitrile	2.01	164
DSSC with TiO ₂ /ZnO nanoflowers and TiO ₂ nanorod array	Chen <i>et al.</i>	Double layered photoanode having an overlayer of a TiO ₂ NR array and underlayer of a TiO ₂ embedded ZnO nanoflower array by a sol–gel method	N719	Lil, I_2 and LiClO $_4$ in acetonitrile	8.01%	185

Table 2 (Contd.)

		Dhotoelectrode and method of				
DSSC Type	Author	preparation	Sensitizer	Electrolyte	Efficiency	Ref.
DSSC with rutile TiO_2 nanorods incorporated with α alumina	Sriharan <i>et al.</i>	Rutile TiO ₂ nanorods incorporated with α alumina were developed on an FTO surface via a hydrothermal route	N719	KI, I ₂ and 4- <i>tert</i> -butyl pyridine	6.5%	186
DSSC with a 3 dimensional hierarchical TiO ₂ nanorod array wrapped with rGO	Subramaniam et al.	Three dimensional hierarchial TiO ₂ nanorod arrays with a layer of rGO wrapping prepared by an <i>in situ</i> hydrothermal method	N719	Li/I_2 in acetonitrile	4.54%	187
DSSC with PANI wrapped rutile TiO_2 nanorods	Roy et al.	Hydrothermal derived rutile TiO ₂ NRs wrapped with an <i>in situ</i> deposited layer of PANI	N719	1-Methylbenzimidazole (NMB) was mixed with a 1:1 volume ratio of acetonitrile and 3-methoxypropionitrile (MPN) solution followed by the addition of LiI, tetrabutylammonium iodide (TBAI), and I ₂	4.28%	188

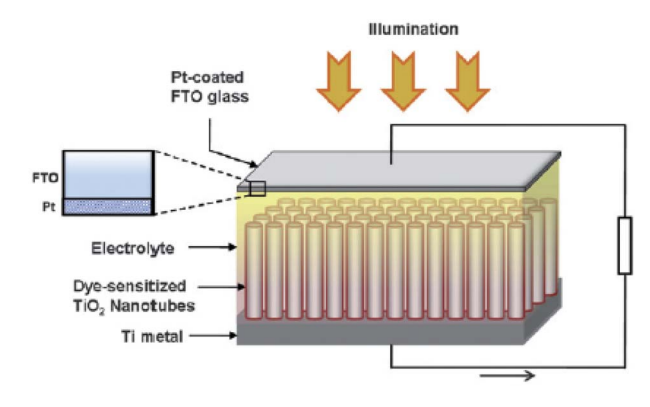
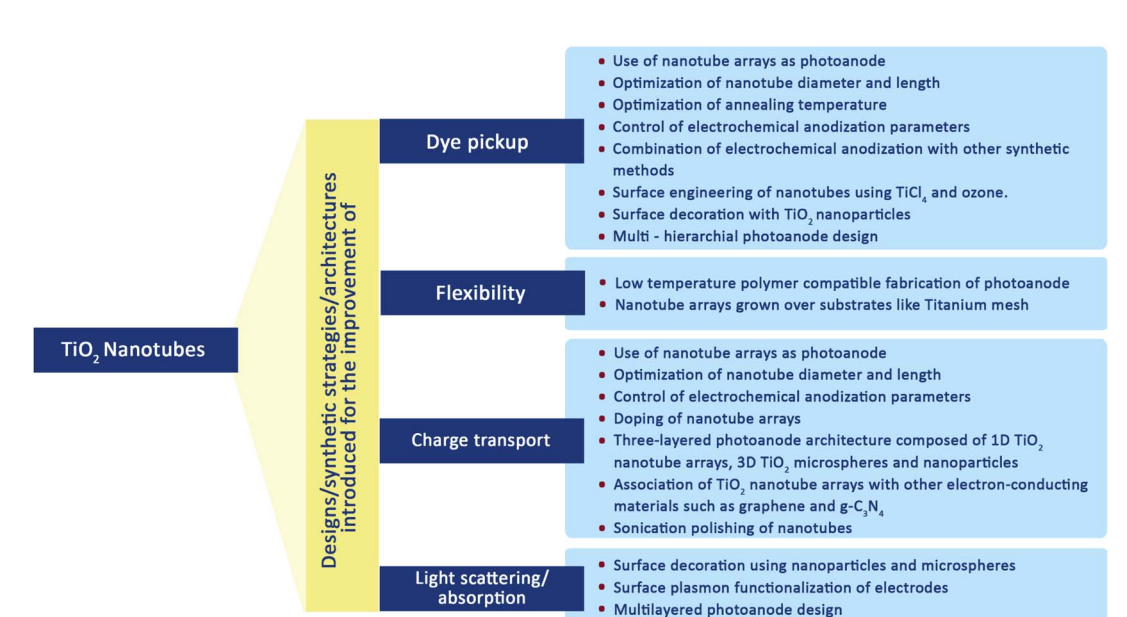


Fig. 14 Schematic representation of typical solar cell construction using ${\rm TiO_2}$ nanotubes grown on a Ti substrate. (Reprinted with permission from ref. Roy *et al.*, 2010. Copyright 2009, Royal Society of Chemistry.)

In 2011 it has been reported that nanorods prepared by the hydrothermal method were used as seeds for the synthesis of a TiO_2 nano-branched photoanode. This nano-branched array has achieved an efficiency of 3.75%.

Efforts were made to make NR-based DSSCs flexible by growing NRs on substrates other than the FTO plate. Such an innovative electrode architecture was introduced by Guo and their team, in which bunched TiO₂ nanorods were grown on carbon fibres by a 'dissolve and grow' method.¹⁷⁷ By using these carbon fibres coated with bunched TiO₂ nanorods, tube-shaped flexible 3D DSSCs have been prepared with an efficiency of 1.28%. Wang *et al.* made a similar attempt for enhancing flexibility by preparing single crystal nanorod assembled TiO₂ cloth from carbon cloth templates. Wang *et al.* employed a rapid microwave heating process for TiO₂ cloth synthesis and this DSSC assembly yielded an efficiency of 2.21%. Wang *et al.* investigated the influence of sensitizers such as N719, C218 and D205 on TiO₂ nanorod array-based photoanodes and found out that the best efficiency is obtained from C218.¹⁷⁸

Also, the performance of TiO₂ NR array DSSCs depends strongly on the annealing temperature. 179,180 Researchers found that annealed nanorod arrays show an improvement of more than 400% in efficiency compared to unannealed NRs. This increase can be attributed to reduced recombination and better electric contact between the NRs and FTO substrate. Efficiency improvement of TiO2 nanorod-based DSSCs can be made by surface modifications such as nanoparticle decoration, 181 chemical etching,182 doping,183 TiCl4 treatment184 etc. Ghaffari et al. showed that the generation of photoelectrons by Au NPs can help electron-hole separation and thereby result in enhanced fill factor (FF) and short circuit current values (I_{sc}) .¹⁸¹ The photochemical reduction process under ultraviolet radiation was employed for loading Au NPs on TiO2 NRs. Yao et al. prepared Nd doped TiO2 NRs by the solvothermal method.183 Here the doped Nd ions enhanced the injection of excited electrons and thereby decreased the electron-hole recombination. The obtained efficiency was 4.4% which is 33.3% greater than that of the undoped analogue.



Scheme 3 Various modifications introduced for the improvement of TiO2 nanotube based DSSC performance.

Later, a combination of TiO_2 nanomorphologies with other nanomaterials gained considerable interest. One such photo-anode material consists of an overlayer of TiO_2 nanorods and an underlayer of TiO_2 embedded ZnO nanoflowers. The double-layered design was introduced by Chen and co-workers and they achieved a photo conversion efficiency of 8.01%. A similar composite design consists of rutile TiO_2 nanorods incorporated with an α alumina thin film. Here α alumina facilitated an enhanced electron lifetime and better charge transport. The α alumina incorporated TiO_2 nanorod arrays exhibited a PCE of 6.5%.

To boost the charge collection efficiency of TiO₂ nanorods, a layer of reduced graphene oxide (rGO) was wrapped over the nanorod surface by Subramaniam and his team. ¹⁸⁷ 2 wt% rGO loaded nanocomposite was found to show a superior photo conversion efficiency of 4.54%. Another effort was made by Roy and co-workers to improve the electron transport which involved the wrapping of rutile TiO₂ nanorod arrays with polyaniline (PANI) on their surface. ¹⁸⁸ Being a conducting polymer, PANI enhanced the electron transport and the conjugation

helped to capture more photoelectrons which in turn diminished the recombination between photo excitons. The association of a TiO₂ NR photoanode with PANI made more visible light absorption possible. Later Tang and co-workers reported that the higher the aspect ratios of TiO₂ NRs, the higher the dye loading capacity and efficiency will be. 189 Here NRs having different aspect ratios were prepared by controlling the reaction time. Also, improved performance of branched TiO₂ NRs was investigated by Hu *et al.* 164. Prominent research on TiO₂ nanorod-based DSSC photoanodes is tabulated in Table 2.

3.3. Nanotubes

TiO₂ nanotubes were introduced with a hollow cavity structure, possessing a higher active surface area. Their enhanced absorption capacity and fast electron transport ability were examined by researchers^{194,195} and they were found suitable for DSSC applications as shown in Fig. 14. Gaps in TiO₂ mesostructures, which act as electron traps, can be avoided by using nanotube arrays having small boundaries in between. This

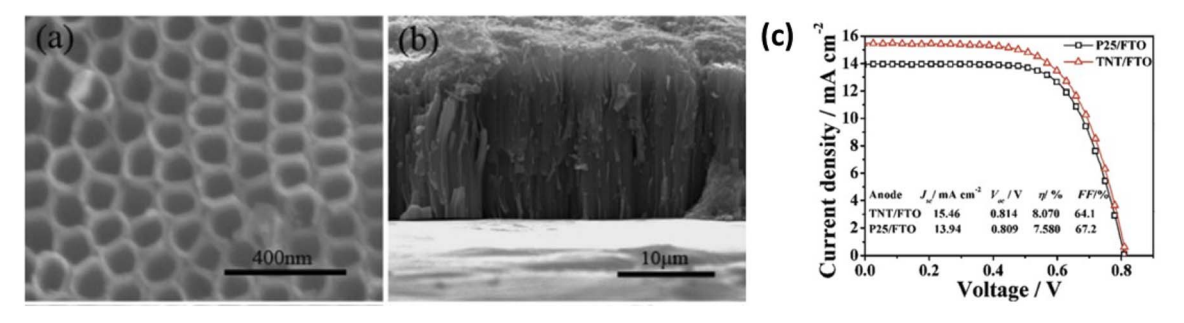


Fig. 15 (a and b) FE-SEM images of as-prepared TNT/Ti arrays. (c) Comparison of photovoltaic performance using the same thickness (20.8 μm) of the TNT/FTO film and P25/FTO film under AM 1.5 G illumination (100 mW cm⁻²).²⁰⁶ (Reprinted with permission from ref. Lei *et al.*, 2010. Copyright 2010 ECS – American Chemical Society.)

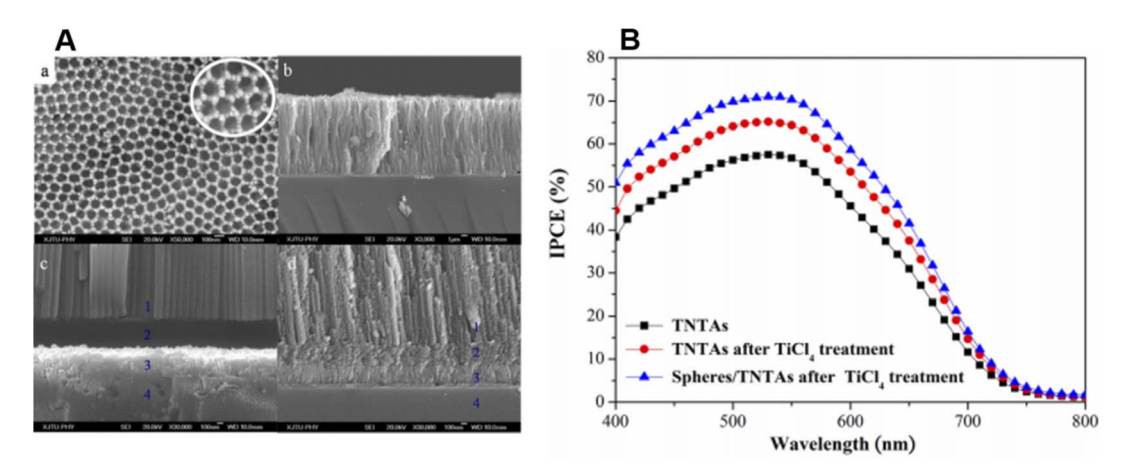


Fig. 16 (A) SEM images of highly ordered TiO_2 nanotube arrays: (a) top view; (b) cross-sectional view; (c) cross-sectional view of the bottom, before $TiCl_4$ treatment; and (d) cross-sectional view of the bottom, after $TiCl_4$ treatment; (B) incident photon-to-current conversion efficiency (IPCE) curves of solar cells based on TNTAs sensitized by N719.²¹⁰ (Reprinted with permission from ref. He *et al.*, 2013.Copyright 2013, American Chemical Society.)

results in an increased diffusion length i.e. the distance travelled by an electron in a tube before recombination. 196 It was estimated that the diffusion length of a nanotube cell is approximately 100 µm. 197 So up to this limit, the tube size can be increased which in turn increases the surface area without promoting recombination. The oxidised species from the electrolyte can easily escape from nanotubes because of their 'open' structure as compared to from the mesoporous layers. Once it is oxidised, it will diffuse towards the cathode and get reduced back rapidly to minimise recombination losses. 198 The drawbacks of TiO₂ nanotubes are their high manufacturing cost and time-consuming preparation techniques. 199 The efficiency of DSSCs employing TiO2 nanotubes is dictated by factors such as morphology and the crystalline structure of the tubes. It is observed that reduction in the tube diameter has a superior role in efficiency compared to the increase in the tube length.²⁰⁰ Also, dye loading depends on the annealing temperature of the nanotubes.200 The next factor is collection efficiency, which can be improved by minimising recombination losses by introducing modifications on the tube surfaces.201,202

Scheme 3 provides an overall idea of the efforts made to improve TiO2 nanotube based photoanode performance in DSSCs. Some of the significant nanotube-based DSSC architectures are discussed in this section. One of the earliest attempts involved the use of nanotube powders formed by a surfactant template-assisted technique.203 These disordered nanotube array has achieved an efficiency of 4.88%.203 The most widely employed technique for nanotube synthesis was electrochemical anodization. 202-208 These electrochemical anodizations were carried out in different electrolytes by different research groups. Yi et al. investigated the influence of parameters like water content, anodization time and post-treatment of nanotubes on the photoconversion efficiency of the photoanodes.209 It is found that efficient systems can be developed out of a combination of anodization with other synthetic methods for the fabrication of hybrid and multi-layered photoanodes. 210-216 Another simpler route of TiO2 nanotube synthesis

proposed by Ramakrishnan and co-workers involved the hydrothermal treatment of quasi-crystalline TiO2 nanoparticles.217 They were reported to have achieved hydrothermal conditions even without using an autoclave. Apart from using individual nanotubes, designs involving nanotube arrays were made by certain research groups. 194,204,206-208,210,212-215,218-220 For example, a highly ordered array of TiO2 nanotubes with a length of 360 nm was introduced in 2006 by Mor and co-workers with a PCE of 2.9%.221 This reduction in PCE is due to the comparatively smaller thickness of the photoelectrode. Mor et al. claimed that the efficiency can be further improved towards the ideal limit of \sim 31% by increasing the length of the nanotube array up to a few micrometres. Wang et al. showed that efficiency can also be increased by treatment of TiO2 nanotube arrays with TiCl₄ and ozone.²⁰² Such a surface engineered TiO₂ nanotube array attained an efficiency of 7.37%. Lei et al. brought the efficiency to 8.07%, employing one dimensional TiO₂ nanotube arrays (Fig. 15a and b) prepared by anodization.206 The I-V plots obtained by Lei and team for the TNT/FTO film in comparison with the P25/FTO film are shown in Fig. 15c. Another report by Hun Park and co-workers shows that TiO₂ nanotubes longer than 15 µm, transplanted on an FTO plate achieved an efficiency of 5.36% after TiCl₄ treatment.²⁰⁷ TiO₂ nanotube arrays were also subjected to doping with other elements.222-224 The intention of adding dopants is to perfectly match the LUMO of dye molecules to the conduction band of TiO2 for efficient electron transfer. This kind of perfect alignment will result in enhanced electron injection and reduced electron recombination. Yang et al. introduced TiO₂ nanotubes doped with Nb by anodizing Ti–Nb alloys ($\eta = 3.21\%$).²²² Using the same technique, So et al. prepared Ru-doped TiO2 nanotubes from Ti-Ru alloys($\eta = 5.16\%$).²²³ While adding metal content it is found that the efficiency is the maximum for an optimum value of metal concentration. Also, metal doping will have an adverse effect if the length of the tubes is not correctly controlled. Subramanian et al. fabricated DSSCs with borondoped TiO2 nanotube arrays.224 Here B doped nanotube arrays

Table 3 TiO₂ nanotube based DSSCs

DSSC TVDe	Author	Photoelectrode and method of	Sensitizer	Electrolyte	Efficiency	Ref.
316					6	
DSSC with TiO ₂ nanotubes	Adachi <i>et al.</i>	Titania nanotubes were synthesized using molecular assemblies	N3	0.03 M iodine in 0.3 M lithium iodide in 3-methyl-2-oxazolidinone (NMO)/ acetonitrile	4.88%	203
DSSC with a TiO ₂ nanotube array	Maggie <i>et al.</i>	Highly ordered TiO ₂ nanotube arrays are made by anodization of a titanium film in a fluoride containing electrolyte	N719	Lil, 1 ₂ , <i>N</i> -methylbenzimidazole, guanidinium thiocyanate, and <i>tert</i> -butylpyridine in methoxypropionitrile (MPN)	4.7%	204
DSSC with TiO ₂ nanotubes decorated with TiO ₂ NPs	Roy et al.	TiO ₂ nanotubes were prepared by anodization of Ti foil followed by annealing and TiCl ₄ treatment	N719	lodolyte R50 (Solaronix)	3.8%	205
DSSC with a ${\rm TiO_2}$ nanotube array	Wang et al.	Highly ordered TiO ₂ nanotube arrays were fabricated by electrochemical anodization followed by surface engineering using TiCl ₄ and O ₂ plasma	N719	BMIM-I, I ₂ , TBP, and GTC in acetonitrile/ valeronitrile	7.37%	202
DSSC with a ZnO nanorod and TiO ₂ nanotube hybrid photoanode	Cirak <i>et al.</i>	Hybrid photoanode with ZnO nanorods and TiO ₂ nanotubes prepared through anodic oxidation followed by hydrothermal deposition	N719	I ⁻ /I ₃ ⁻ redox pair (Hi-30, Solaronix)	1.67%	228
DSSC with a ${\rm TiO_2}$ nanotube array	Lei <i>et al.</i>	Highly ordered one-dimensional TiO_2 nanotube arrays were prepared by anodization of pieces of Ti foil	N719	I ₂ , 1-methyl-3-propylimidazolium iodide (PMII), guanidinium thiocyanate, and <i>tert</i> -butylpyridine in acetonitrile and valeronitrile	8.07%	206
DSSC with TiO ₂ nanotube arrays	Park <i>et al.</i>	Highly ordered TiO ₂ nanotube arrays were fabricated by anodization and transplanted on to an FTO substrate	N719	1-Hexyl-2,3-dimethyl-imidazolium iodide (C6DMIm), iodine (I ₂), lithium iodide (LiI), and 4-tert-butylpyridine in 3-methoxypropionitrile	5.36%	207
DSSC with Nb doped TiO ₂ nanotube layers	Yang et al.	Nb-doped TiO ₂ nanotube layers were prepared by electrochemical anodization of Ti-Nb alloys	N719	I_3^-/I^- as the redox electrolyte	3.21%	222
DSSC with a TiO ₂ nanotube array/NPs	Zheng <i>et al.</i>	Layer-by-layer assembly of self-standing titania nanotube arrays and NPs were prepared by anodization	Ru535-bisTBA	1,2-dimethyl-3-propyl imidazolium iodide, Lif, 1 ₂ , and <i>4-tert</i> -butylpyridine in acetonitrile	8.80%	208
DSSC with Ru doped ${\rm TiO}_2$ nanotubes	So et al.	Ru doped TiO ₂ nanotubes were prepared by anodization of Ti-Ru alloys	D-719, (Eversolar, Taiwan)	Iodolyte R50 (Solaronix)	5.16%	223
DSSC with B doped TiO ₂ nanotube arrays (TNAs)	Subramanian <i>et al.</i>	B doped TiO ₂ nanotubes were prepared by anodization of Ti foil in the presence of 0.5 wt% NH ₄ F and 5 wt% 0.5 M boric acid in ethylene glycol solution	N719	Iodolyte R-150	3.44%	224

_
₹
+
C
7
્
٧
0
7
-
2

DSSC Type	Author	Photoelectrode and method of preparation	Sensitizer	Electrolyte	Efficiency	Ref.
DSSC with TiO ₂ nanotubes and TiO ₂ microspheres	He et al.	TNTAs were prepared by anodization of pieces of Ti foil in an aqueous solution containing hydrofluoric acid and TiO ₂ scattering microspheres were prepared via a microwave solvothermal process	N719	I ₂ , 1-methyl-3-propylimidazolium iodide (PMII), guanidinium thiocyanate, and <i>tert</i> -butylpyridine in a solution of valeronitrile and acetonitrile	7.24%	210
DSSC with a TiO ₂ nanotube photoelectrode and transparent Pt counter electrode	Lee et al.	Ti layers deposited over an FTO substrate were completely anodized to obtain TiO ₂ nanotubes	D-719, Eversolar, Taiwan	Iolilyt SB-163(Iolitec, Germany)	7.58%	230
DSSC with TiO ₂ nanotube/ microsphere/NPs tri-layered photoanode	Wu et al.	Double layered photoanode with a 1D NT underlayer and 3D hierarchical upper layer was prepared by a hydrothermal method and then incorporated with hydrothermally prepared 7iO, NPs	N719	1-Methyl-3-propylimidazo-lium iodide (PMII), guanidinium thiocyanate, I ₂ , LiI, and <i>tert</i> -butylpyridine dissolved in acetonitrile and valeronitrile	9.10%	211
DSSC with an open ended TiO ₂ nanotube array	Hou et al.	Vertically oriented, high-aspect-ratio TNT arrays were prepared by two-step anodic oxidation	N719	1-Methyl-3-propylimidazo-lium iodide (PMII), guanidinium thiocyanate, I ₂ , Lil, and tert-buylpyridine dissolved in acetonitrile and valeronitrile	5.01%	220
DSSC with cone shaped TiO ₂ nanotube arrays	So et al.	Cone shaped TiO ₂ nanotubes were prepared by anodization followed by TiCl, treatment	N719	BMIM-I, I ₂ , and GTC in acetonitrile/ valeronitrile (SB-163, IoLiTec Inc, Germany)	%8	231
DSSC with TiO ₂ nanotube arrays	Gu et al.	TiO ₂ NTAs were synthesized by a modified electrochemical anodic oxidation method <i>i.e.</i> sonication followed by anodization. Then the nanotubes were filled with $8b_2S_3$ by chemical bath denosition	N719	Lif, I ₂ , and <i>tert</i> butylpyridine in acetonitrile	6.28%	212
DSSC with a composite of P25 NP/TiO ₂ NTA/flower like TiO ₂	Hu et al.	TiO ₂ NTAs prepared by anodization were transplanted on to a P25 coated FTO plate and then flower like TiO ₂ prepared hydrothermally was deposited over a P25/NTA film	N719	Lil, I ₂ , 4-tert-butylpyridine and 1, 2-dimethyl-3-propylimidazolium iodide (DMPII) in dry acetonitrile	6.48%	213
DSSC with Ag nanoparticle- Functionalized open-ended freestanding TiO ₂ nanotube	Rho et al.	TiO2 nanotube arrays prepared by anodization, with channels containing Ag NPs coated with TiO2 NPs for light scattering	N719	I ₂ , guanidium thiocyanate (GSCN), and 4- tert-butylpyridine (TBP) in a mixture of acetonitrile and valeronitrile	7.05%	214
Darty 2 Darty 2 Darty TiO ₂ nanoparticle photoanode	Fu <i>et al.</i>	"Cigar-like" Au/TiO ₂ -nanotube-array/ TiO ₂ -nanoparticle multi-hierarchical photoanode through a novel vacuum- assisted colloid-filling approach	N719	Lil, 1 ₂ , 1-methyl-3-hexylimidazolium iodide (HMII), <i>N</i> -methylbenzimidazole (NMB) and <i>4-tert</i> -butylpyridine in 3- ethoxypropionitrile	8.93%	227
DSSC with TiO ₂ nanotube arrays	Peighambardoust et al.	Pieces of Ti foil were degreased ultrasonically and then anodized to form TiO ₂ NTAs	N719	Ionic-salt-based liquid electrolyte	3.14%	215

DSSC Type	Author	Photoelectrode and method of preparation	Sensitizer	Electrolyte	Efficiency	Ref.
DSSC with a tri-layered photoanode	Wu et al.	Tri-layered photoanode consisting of single crystal hollow TiO ₂ nanoparticles (HTNPs), sub-micro hollow TiO ₂ mesospheres (SHTMSs) and hierarchical TiO ₂ microsuberes (HTMSs)	N719	1-Methyl-3-propylimidazo-lium iodide (PMII), guanidinium thiocyanate, I ₂ , LiI, and <i>tert</i> -butylpyridine dissolved in acetonitrile and valeronitrile	9.24%	216
DSSC with an open ended TiO ₂ nanotube array photoanode	Zhu et al.	Open ended TiO ₂ nanotube array photoanode was prepared by fast removal of bottom caps by mechanical ball milling	N719	Lil, I ₂ , 1-methyl-3- hexylimidazolium iodide (HMII), <i>N</i> -methylbenzimidazole (NMB), and 4-tert-butylpyridine in 3- methoxypropionitrile	7.7%	232
DSSC with a single layer graphene–TiO ₂ nanotube array heterojunction	Wang et al.	Single layer graphene-TiO ₂ nanotube array heterojunction photoanode synthesized by a wet transfer method	N719	Ethylene glycol solution containing NH_4F and H_2O	4.18%	229

were prepared by anodization and they achieved an efficiency of 3.44% with an increased electron lifetime and reduced interface resistance. Besides doping, surface decoration with NPs and microspheres was also tried by different groups. 205,208,210,214 Roy et al. observed that appropriate treatment of NTAs with TiCl₄ will result in the decoration of the NTA surface with TiO2 nanocrystals.205 Such decorations enhanced dye pick up and thereby improved efficiency. He et al. decorated a TiO2 NTA with TiO₂ microspheres synthesized by a microwave solvothermal process which yielded an efficiency of 7.24%.210 Fig. 16 shows SEM images as well as I-V characteristics of He's photoelectrode. Rho et al. introduced open-ended free-standing TiO₂ NTAs functionalized by Ag NPs and coated by TiO2 NPs.214 Here nanotube channels were functionalized with Ag NPs to create a plasmonic effect. At the same time, TiO₂ NPs facilitate scattering. A combination of both these effects resulted in an efficiency of 7.05%. A similar plasmonic enhancement of power conversion efficiency was achieved with the incorporation of Au nanoparticles into TiO2 nanotube arrays by Chen et al.225 The obtained 19% improvement in PCE for the Au nanoparticle inlaid TNT arrays can be attributed to the surface plasmon resonance and scattering effect of the incorporated Au nanoparticles. In the same year, Guo and co-workers came up with a novel single-photon management architecture for a DSSC photoanode.²²⁶ Their design, consisting of a TiO₂ nanotube photonic crystal deposited with Au nanoparticles, achieved a PCE of 5.63% which was the result of the synergistic effect of a photonic crystal and surface plasmon resonance of Au nanoparticles. Followed by this, in 2019, Fu et al. developed a cigarlike Au/TiO2 nanotube array/TiO2 nanoparticle multi-hierarchical photoanode with a PCE of 8.93%.227 The multi-hierarchical design, which was obtained via a novel vacuum-assisted colloid filling route has 4 times better charge transport and 3.2 times better dye intake than that of the conventional TiO2 nanotube array-based photoanodes. Cirak and co-workers proposed a hybrid photoanode design comprising ZnO nanorods and TiO₂ nanotubes.²²⁸ The hybrid photoanode fabrication was carried out by a two-step synthetic process, anodic oxidation of TiO2 nanotubes followed by hydrothermal deposition of ZnO nanorods over the TiO2 nanotubes. They found the hydrothermal treatment temperature to be a determining factor of PCE. The hybrid design attained a PCE almost double that of the normal TiO₂ nanotube photoanode. As part of achieving increased dye pick up and enhanced light scattering, multilayered photoanode architectures involving TiO2 nanotubes were also introduced. 208,210,211,213,214,216 As mentioned in the case of nanowires and nanorods (Sections 1.8 and 1.9), here also specific functions were assigned to individual layers. In 2014 Wu et al. introduced a three-layered photoanode architecture composed of 1D TiO₂ nanotube arrays, 3D TiO₂ microspheres and zero dimensional nanoparticles.211 This novel structure has inherent properties such as high dye loading capability, efficient light scattering capacity and enhanced charge collection ability, leading to an unprecedented increase in photoconversion efficiency i.e., 9.10%. Later several other research groups fabricated such tri-layered photoanodes with various modifications.213,216

Nanoscale Advances Review

Several other associations of TiO2 nanotube arrays with other electron-conducting materials such as graphene and g-C₃N₄ were later introduced. Wang et al. fabricated a single-layer graphene/TiO2 nanotube array heterojunction photoanode by a wet transfer method and achieved a photon to current conversion efficiency of 4.18% which is far higher than that of pristine TiO2 nanotube photoanodes.229 The formation of a heterojunction with graphene not only reduced the bandgap but also enhanced visible light absorption. Mohammadi and coworkers modified TiO2 nanotube arrays with g-C3N4 and ZnO nanoparticles through a hydrothermal route. Even though there is no significant improvement in PCE by this composite formation, the I_{sc} and V_{oc} of the hybrid photoanode showed considerable improvement. In addition to the above-mentioned investigations, some distinct approaches were also attempted by researchers. For example, Lee et al. investigated the influence of various types of glass substrates on the performance of DSSCs fabricated from TiO2 nanotubes.230 They found that the photoconversion efficiency shows a significant increase with an increase in the conductivity of the glass used. Apart from the conventional cylindrical-shaped nanotubes, So et al. fabricated cone-shaped TiO₂ nanotube arrays with improved photon management capability.231 When used in back side illuminated DSSCs, nanocone structures exhibited efficiencies near 8% which is the highest efficiency reported for this type of DSSC. Later in 2014, open-ended TiO2 nanotubes prepared by electrochemical anodization of Ti foil were used for DSSC fabrication by Hou et al. and these DSSCs were subjected to stability studies by I-V characterisation.²²⁰ Their results indicate that the PCE decay of the DSSCs depends on the $J_{\rm sc}$, instead of the $V_{\rm oc}$ and FF, with the extension of testing time. The stability of DSSCs mainly depends on the sealing properties and the volatile electrolyte of the devices. In 2016 Gu et al. reported the removal of the capping layer over the TiO2 nanotubes and subsequent enhancement of charge transport by sonication polishing treatment.212 This sonication polishing helped the removal of flocculent substances atop TiO2 nanotube arrays (NTAs) and also smoothened their outer surface. They have obtained an efficiency of 6.28%. Zhu et al. synthesized openended TiO2 nanotube arrays by removing the closed bottom caps by ball milling.232 The fast ball removal of bottom caps enhanced their surface area and the open-ended photoanode exhibited a PCE of 7.7%. As a generalisation, the common modification strategies of TiO₂ nanotubes include (a) attaching light-harvesting molecules i.e. sensitization of nanotubes, 206,215 (b) doping, 218,222-224,233 (c) band gap engineering, 202 (d) inducing electronic heterojunctions^{204,219,234} and (e) secondary semiconductor particle decoration.205 An overview of DSSC applications of the tubular morphology of TiO2 nanomaterials is given in Table 3.

3.4. Effect of one-dimensional nanomaterial morphology on electronic and charge transport properties

Compared to bulk TiO2 having a wide bandgap, one dimensional TiO2 nanostructures exhibited enhanced surface area, more active sites and quantum confinement effects. Size, specific crystal facets, morphology and alignment are the main factors determining the electronic properties of these one dimensional TiO2 structures. In the case of nanowires, as the size reduces to the nanoscale regime, the bandgap starts increasing as per quantum confinement.66 Doping of foreign elements is the main strategy employed for the tuning of the bandgap and such dopants can align the valence band and conduction band positions in favour of the sensitizer energy levels. Also, the best DSSC performances were obtained for vertically aligned nanowire based photoanodes. In the case of nanorods, significant reduction in grain boundaries which act as electron traps caused an increment in the electron diffusion length and thereby enhanced charge transfer. 174,178 The bandgap adjustment can be made in TiO2 nanorods by varying the aspect ratio of nanorods. With an increase in the aspect ratio of nanorods, there will be a downshift of the conduction band edge. 66 Similarly, surface area enhancement can be achieved by introducing surface roughness and mesoporosity.235 In the case of TiO2 nanotubes, those having a wall thickness less than 5 nm are capable of manifesting quantum confinement effects.²³⁶ Only hydrothermal tubes fall under this category. The presence of Ti³⁺ and oxygen vacancies are another reason for enhanced charge transport. Annealing temperature is a crucial factor determining the charge transport ability of nanotubes.236 Bandgap engineering in nanotubes can be made by doping, surface adsorption, heterojunction formation and surface decoration. 76,205,222,223

3.5. Significance of one-dimensional TiO₂ nanomorphology for exploitation of the photoanode performance

TiO₂ one-dimensional (1D) morphologies were introduced as photoanode materials to overcome the limitations encountered by TiO2 nanoparticulate electrodes. These one-dimensional morphologies are found to have profound photoelectrode characteristics with certain constraints which limit their use as photoanodes. We address this problem to highlight a particular one-dimensional morphology as the best choice by analysing various TiO2 nanomaterials with 1D morphologies. A clear distinction of the best among nanowires, nanorods and nanotubes as photoanode materials requires a detailed investigation of several aspects. The main aspects to be considered are the band gap, surface area, aspect ratio, charge recombination time, transport properties and stability. In terms of surface area, nanowires, nanorods and nanotubes are inferior to zerodimensional TiO2 nanoparticles.89 However, they possess high aspect ratios and better charge transport pathways compared to conventional multidimensional TiO2 NPs. As a result of limited surface area, the amount of dye (sensitizer) intake into these one-dimensional morphologies would be lesser. Even then, DSSCs based on TiO₂ one-dimensional photoanodes exhibit better IPCEs. It was found that the TiO₂ NP layer, having thrice the surface area of a TiO₂ nanotube layer, exhibited a much lower IPCE compared to the nanotube layer.237 This enhancement in IPCE of nanotubes can be attributed to the much larger electron transport time prevailing in them.237 In the case of nanotube photoanode materials, the fraction of dye intake as

well as electron diffusion lengths increases with an increase in the tube length. The electron diffusion lengths in nanotubes are almost thirty times that of NPs.236,237 Thus, an increased tube length can have the synergic effect of both surface area enhancement and smoother electron transport, irrespective of the high density of electron trap states in TiO₂ nanotubes. Similar results are obtained in the case of TiO₂ nanowires also. The best efficiencies are obtained upon arranging the nanowires vertically rather than randomly, which ensures effective contact between individual nanowires and the electrode.66 With an increase in the length of nanowires, the number of electron traps and dye loading increases. So, finding the optimal nanowire length ensures the best IPCE. The TiO2 nanorod-based photoanode exhibited an electron lifetime 8 times that of a TiO₂ NP-based one.174 TiO2 nanorods showed increased electron diffusion lengths and reduced grain boundaries compared to NP-based electrodes. 191 The above information leads us to the conclusion that the selection of the best one-dimensional TiO₂ photoanode material among the three i.e., nanorods, nanowires and nanotubes is rather difficult. This dilemma arises due to the vast number of modifications possible over one dimensional TiO₂ nanomaterials using various design strategies under different experimental conditions. Several of these investigations have led to significant and valuable findings regarding the photoanode architecture, performance parameters and stability. Upon a detailed survey of the literature, it can be seen that the combination of one dimensional TiO2 nanomaterials with other nanomaterials exhibited the best conversion efficiencies. These nanomaterials are chosen in such a way that the limitations of one-dimensional TiO2 morphologies can be made up by them. Particle decoration, heterojunction formations and multi-layered architectures are superior design strategies employed for the fabrication of modified onedimensional TiO2 photoanodes. The limited surface area of the one-dimensional structures is improved by the addition of TiO2 NPs. These added layers cause enhanced light scattering and better dye loading capability. Decoration with metal nanoparticles makes use of surface plasmon resonance and yields better light absorption and electron transport. Heterostructures of one-dimensional TiO2 with materials having suitable band structures and electron transport properties exhibit improved efficiency. From the above literature survey (Tables 1, 2 and 3), it

4. Summary and future prospects

and hydrothermal methods yield higher efficiencies.

This review discusses the design and working principle of various TiO2 nanomorphologies and surveys various aspects of TiO₂ based photoanode materials in dye-sensitized solar cells. The total reliance of mankind on non-renewable energy sources

can be seen that top IPCE values were obtained for multi-layered

photoanodes involving one-dimensional TiO2 morphologies.

Each layer was incorporated with a specific function to be

carried out, and such a division of labour led to enhanced

outputs. Single layered one-dimensional TiO2 morphologies

prepared by advanced techniques like electrospinning, anod-

ization, etc. or a combination of these techniques with sol-gel

has resulted in their depletion as well as serious environmental pollution. In this scenario, sunlight is considered a universal source of energy which is abundant in nature and free of cost. Thus, solar energy and its conversion into electricity and fuel (hydrogen) can be exploited. Solar cells which convert sunlight into electricity can be considered a future remedy for the energy crisis. In recent years a wide variety of TiO2 nanostructures have been synthesized as photoanodes for DSSC applications such as nanoparticles, nanowires, nanorods, nanotubes, etc. Due to their excellent scattering ability and high electron transport rate, these one-dimensional nanostructures are found to be efficient candidates for DSSC photoanode fabrication. By overcoming their limitations with surface area, even higher efficiencies can be achieved. The suitable band alignment of TiO2 with the sensitizer and the subsequent charge transport properties make it more attractive among other semiconductors in addition to its non-toxicity and viable functional architecture. TiO₂ nanomaterials have a band gap in the UV region of solar spectra which restricts their use in the field of visible active applications. In DSSCs, the electrons in the LUMO of the dye are transferred to the conduction band of TiO2 nanomaterials. Anion and cation doping in TiO2 nanomaterials are remarkable routes to make suitable alignments of the LUMO of the dye and conduction band position of TiO2 for fast electron transfer. Recent reports show that the IR absorption capability of TiO2 can be enhanced by extending its absorption edge into the infrared region which provides a high charge collection. 116,238

Conflicts of interest

There are no conflicts to declare.

References

- 1 M. Van der Hoeven, World energy outlook 2013, International Energy Agency, Tokyo, Japan, 2013.
- 2 B. Petroleum, bp. com/statisticalreview, BP, London, 2012.
- 3 BP statistical review of world energy, B. Petroleum, British Petroleum, London, UK, 2018.
- 4 J. Zhao, A. Wang, M. A. Green and F. Ferrazza, Appl. Phys. Lett., 1998, 73, 1991-1993.
- 5 H. Garg, in Advances in Solar Energy Technology, Springer, 1987, pp. 279-383.
- 6 M. A. Green, Y. Hishikawa, W. Warta, E. D. Dunlop, D. H. Levi, J. Hohl-Ebinger and A. W. Ho-Baillie, Prog. Photovolt.: Res. Appl., 2017, 25, 668-676.
- 7 S. Yoon, T. Yoon, K.-S. Lee, S. Yoon, J. M. Ha and S. Choe, Sol. Energy Mater. Sol. Cells, 2009, 93, 783-788.
- 8 T. Suntola, MRS Bull., 1993, 18, 45-47.
- 9 P. Jackson, D. Hariskos, E. Lotter, S. Paetel, R. Wuerz, R. Menner, W. Wischmann and M. Powalla, Prog. Photovolt.: Res. Appl., 2011, 19, 894-897.
- 10 M. A. Contreras, B. Egaas, K. Ramanathan, J. Hiltner, A. Swartzlander, F. Hasoon and R. Noufi, Prog. Photovolt.: Res. Appl., 1999, 7, 311-316.
- 11 M. Grätzel, J. Photochem. Photobiol. C: Photochem. Rev., 2003, 4, 145-153.

Nanoscale Advances

- 12 G. Korotcenkov, The Future of Semiconductor Oxides in Next-Generation Solar Cells, Elsevier, 2017.
- 13 M. Freitag, J. Teuscher, Y. Saygili, X. Zhang, F. Giordano, P. Liska, J. Hua, S. M. Zakeeruddin, J.-E. Moser and M. Grätzel, Nat. Photonics, 2017, 11, 372-378.
- 14 J. Gong, K. Sumathy, Q. Qiao and Z. Zhou, Renewable Sustainable Energy Rev., 2017, 68, 234-246.
- 15 B. O'regan and M. Grätzel, Nature, 1991, 353, 737-740.
- 16 K. Kakiage, Y. Aoyama, T. Yano, K. Oya, J.-i. Fujisawa and M. Hanaya, Chem. Commun., 2015, 51, 15894-15897.
- 17 S. Zhang, Study of fluorine-doped tin oxide (FTO) thin films for photovoltaics applications, Université Grenoble Alpes, ComUE, 2017.
- 18 A. Muthukumar, G. Rey, G. Giusti, V. Consonni, E. Appert, H. Roussel, A. Dakshnamoorthy and D. Bellet, AIP Conf. Proc., 2013, 1512, 710-711.
- 19 S. Agarwala, M. Kevin, A. Wong, C. Peh, V. Thavasi and G. Ho, ACS Appl. Mater. Interfaces, 2010, 2, 1844-1850.
- 20 Y. Tang, X. Pan, C. Zhang, S. Dai, F. Kong, L. Hu and Y. Sui, I. Phys. Chem. C, 2010, 114, 4160-4167.
- 21 J. W. Ondersma and T. W. Hamann, Coord. Chem. Rev., 2013, 257, 1533-1543.
- 22 G. Boschloo and A. Hagfeldt, Acc. Chem. Res., 2009, 42, 1819-1826.
- 23 C. H. Yoon, R. Vittal, J. Lee, W.-S. Chae and K.-J. Kim, Electrochim. Acta, 2008, 53, 2890-2896.
- 24 Z. Tang, J. Wu, M. Zheng, J. Huo and Z. Lan, Nano Energy, 2013, 2, 622-627.
- 25 K. Hara and S. Mori, Handbook of photovoltaic science and engineering, 2010, 642-674.
- 26 V. Sugathan, E. John and K. Sudhakar, Renewable Sustainable Energy Rev., 2015, 52, 54-64.
- 27 M. Grätzel, J. Photochem. Photobiol., A, 2004, 164, 3–14.
- 28 M. A. Green, Solid-State Electron., 1981, 24, 788-789.
- 29 Z. Chen, T. G. Deutsch, H. N. Dinh, K. Domen, K. Emery, A. J. Forman, N. Gaillard, R. Garland, C. Heske and T. F. Jaramillo, in *Photoelectrochemical Water Splitting*, Springer, 2013, pp. 87-97.
- 30 M. A. Green, K. Emery, Y. Hishikawa, W. Warta and E. D. Dunlop, *Prog. Photovolt.: Res. Appl.*, 2015, 23, 1–9.
- 31 K. Zhu, N. Kopidakis, N. R. Neale, J. van de Lagemaat and A. J. Frank, J. Phys. Chem. B, 2006, 110, 25174-25180.
- 32 J. Kumari, N. Sanjeevadharshini, M. Dissanayake, G. Senadeera and C. Thotawatthage, Ceylon J. Sci., 2016, **45**, 33-41.
- 33 V. Thavasi, V. Renugopalakrishnan, R. Jose S. Ramakrishna, Mater. Sci. Eng., R, 2009, 63, 81-99.
- 34 F. De Angelis, S. Fantacci and A. Selloni, Nanotechnology, 2008, 19, 424002.
- 35 P. Wang, S. M. Zakeeruddin, R. Humphry-Baker, J. E. Moser and M. Grätzel, Adv. Mater., 2003, 15, 2101-2104.
- 36 D. Chen, F. Huang, Y.-B. Cheng and R. A. Caruso, Adv. Mater., 2009, 21, 2206-2210.
- 37 K. Zhu, N. R. Neale, A. Miedaner and A. J. Frank, Nano Lett., 2007, 7, 69-74.
- 38 P. J. Cameron and L. M. Peter, J. Phys. Chem. B, 2003, 107, 14394-14400.

- 39 J. B. Baxter and E. S. Aydil, Appl. Phys. Lett., 2005, 86, 053114.
- 40 C. Jiang, X. Sun, G. Lo, D. Kwong and J. Wang, Appl. Phys. Lett., 2007, 90, 263501.
- 41 W. Chen, H. Zhang, I. M. Hsing and S. Yang, Electrochem. Commun., 2009, 11, 1057-1060.
- 42 F. Xu and L. Sun, Energy Environ. Sci., 2011, 4, 818-841.
- 43 R. Ghosh, M. K. Brennaman, T. Uher, M.-R. Ok, E. T. Samulski, L. McNeil, T. J. Meyer and R. Lopez, ACS Appl. Mater. Interfaces, 2011, 3, 3929-3935.
- 44 J. Z. Ou, R. A. Rani, M.-H. Ham, M. R. Field, Y. Zhang, H. Zheng, P. Reece, S. Zhuiykov, S. Sriram and M. Bhaskaran, ACS Nano, 2012, 6, 4045-4053.
- 45 H. Zhang, Y. Wang, D. Yang, Y. Li, H. Liu, P. Liu, B. J. Wood and H. Zhao, Adv. Mater., 2012, 24, 1598-1603.
- 46 C. Prasittichai and J. T. Hupp, J. Phys. Chem. Lett., 2010, 1, 1611-1615.
- 47 E. Ramasamy and J. Lee, J. Phys. Chem. C, 2010, 114, 22032-22037.
- 48 H. Song, K.-H. Lee, H. Jeong, S. H. Um, G.-S. Han, H. S. Jung and G. Y. Jung, Nanoscale, 2013, 5, 1188-1194.
- 49 C. W. Kim, S. P. Suh, M. J. Choi, Y. S. Kang and Y. S. Kang, J. Mater. Chem. A, 2013, 1, 11820-11827.
- 50 Y. S. Wang, T. T. Chen, Y. J. Huang, T. P. Huang, Y. Y. Lee, H. T. Chiu and C. Y. Lee, J. Chin. Chem. Soc., 2013, 60, 1437-1441.
- 51 H. Zheng, Y. Tachibana and K. Kalantar-zadeh, Langmuir, 2010, 26, 19148-19152.
- 52 N. Prabhu, S. Agilan, N. Muthukumarasamy and T. Senthil, J. Mater. Sci.: Mater. Electron., 2014, 25, 5288-5295.
- 53 M. Rashad and A. Shalan, Appl. Phys. A, 2014, 116, 781-788.
- 54 B. Tan, E. Toman, Y. Li and Y. Wu, J. Am. Chem. Soc., 2007, 129, 4162-4163.
- 55 J. Chen, L. Lu and W. Wang, J. Phys. Chem. C, 2012, 116, 10841-10847.
- 56 D. W. Kim, S. S. Shin, I. S. Cho, S. Lee, D. H. Kim, C. W. Lee, H. S. Jung and K. S. Hong, Nanoscale, 2012, 4, 557-562.
- 57 S. Yang, Y. Hou, J. Xing, B. Zhang, F. Tian, X. H. Yang and H. G. Yang, Chem.-Eur. J., 2013, 19, 9366-9370.
- 58 A. R. Tanyi, P. Ekanayake, A. L. Tan, D. J. Young and D. Peiris, 2016.
- 59 D. Zheng, J. Xiong, P. Guo, Y. Li and H. Gu, J. Nanosci. Nanotechnol., 2016, 16, 613-618.
- 60 L. De Marco, D. Calestani, A. Qualtieri, R. Giannuzzi, M. Manca, P. Ferro, G. Gigli, A. Listorti and R. Mosca, Sol. Energy Mater. Sol. Cells, 2017, 168, 227-233.
- 61 I. C. Maurya, A. K. Gupta, P. Srivastava and L. Bahadur, J. Solid State Electrochem., 2017, 21, 1229-1241.
- 62 H. Sun, L. Sun, T. Sugiura, M. S. White, P. Stadler, N. S. Sariciftci, A. Masuhara and T. Yoshida, Electrochemistry, 2017, 85, 253-261.
- 63 R. K. Chava and M. Kang, Improving the photovoltaic conversion efficiency of ZnO based dye sensitized solar cells by indium doping, J. Alloys Compd., 2016, 692, 67-76.
- 64 X. Bokhimi, A. Morales, M. Aguilar, J. A. Toledo-Antonio and F. Pedraza, Int. J. Hydrogen Energy, 2001, 26, 1279-1287.

65 M. Posternak, A. Baldereschi and B. Delley, Structural and Electronic Properties of Monoclinic TiO₂ (B) Polymorph, 2007.

- 66 X. Wang, Z. Li, J. Shi and Y. Yu, Chem. Rev., 2014, 114, 9346-9384.
- 67 M. Kapilashrami, Y. Zhang, Y.-S. Liu, A. Hagfeldt and J. Guo, Chem. Rev., 2014, 114, 9662-9707.
- 68 D. Reyes-Coronado, G. Rodríguez-Gattorno, M. E. Espinosa-Pesqueira, C. Cab, R. d. Coss and G. Oskam, Nanotechnology, 2008, 19, 145605.
- 69 M. Shakeel Ahmad, A. K. Pandey and N. Abd Rahim, Renewable Sustainable Energy Rev., 2017, 77, 89-108.
- 70 Y. Hao, Y. Saygili, J. Cong, A. Eriksson, W. Yang, J. Zhang, E. Polanski, K. Nonomura, S. M. Zakeeruddin, M. Grätzel, A. Hagfeldt and G. Boschloo, ACS Appl. Mater. Interfaces, 2016, 8, 32797-32804.
- Madhusudan Reddy, S. V. 71 K. Manorama A. Ramachandra Reddy, Mater. Chem. Phys., 2003, 78, 239-245.
- 72 A. K. Chandiran, M. Abdi-Jalebi, M. K. Nazeeruddin and M. Grätzel, ACS Nano, 2014, 8, 2261-2268.
- 73 E. C. Muniz, M. S. Góes, J. J. Silva, J. A. Varela, E. Joanni, R. Parra and P. R. Bueno, Ceram. Int., 2011, 37, 1017-1024.
- 74 I. S. Cho, Z. Chen, A. J. Forman, D. R. Kim, P. M. Rao, T. F. Jaramillo and X. Zheng, Nano Lett., 2011, 11, 4978-4984.
- 75 X. Feng, K. Shankar, O. K. Varghese, M. Paulose, T. J. Latempa and C. A. Grimes, Nano Lett., 2008, 8, 3781-3786.
- 76 P. Roy, D. Kim, K. Lee, E. Spiecker and P. Schmuki, Nanoscale, 2010, 2, 45-59.
- 77 M. Sabet, M. Salavati-Niasari and O. Amiri, Electrochim. Acta, 2014, 117, 504-520.
- 78 R. L. Z. Hoye, K. P. Musselman and J. L. MacManus-Driscoll, APL Mater., 2013, 1, 060701.
- 79 B. Roose, S. Pathak and U. Steiner, Chem. Soc. Rev., 2015, 44, 8326-8349.
- 80 H. Zhang and J. F. Banfield, Chem. Rev., 2014, 114, 9613-
- 81 T. Umebayashi, T. Yamaki, H. Itoh and K. Asai, J. Phys. Chem. Solids, 2002, 63, 1909-1920.
- 82 M. A. Barakat and R. Kumar, Photocatalytic Activity Enhancement of Titanium Dioxide Nanoparticles: Degradation of Pollutants in Wastewater, Springer International Publishing, 2015.
- 83 F. De Angelis, S. Fantacci, A. Selloni, M. K. Nazeeruddin and M. Grätzel, J. Phys. Chem. C, 2010, 114, 6054-6061.
- 84 S. Meng and E. Kaxiras, Nano Lett., 2010, 10, 1238-1247.
- 85 J. C. Yu, J. Yu, W. Ho, Z. Jiang and L. Zhang, Chem. Mater., 2002, 14, 3808-3816.
- 86 A. A. Murashkina, P. D. Murzin, A. V. Rudakova, V. K. Ryabchuk, A. V. Emeline and D. W. Bahnemann, J. Phys. Chem. C, 2015, 119, 24695-24703.
- 87 M.-J. Jeng, Y.-L. Wung, L.-B. Chang and L. Chow, Int. J. Photoenergy, 2013, 2013, 9.
- 88 X. Hua, Z. Liu, P. G. Bruce and C. P. Grey, J. Am. Chem. Soc., 2015, 137, 13612-13623.

- 89 M. Ge, C. Cao, J. Huang, S. Li, Z. Chen, K.-Q. Zhang, S. S. Al-Devab and Y. Lai, *J. Mater. Chem. A*, 2016, 4, 6772–6801.
- 90 A. Lamberti, A. Sacco, S. Bianco, D. Manfredi, F. Cappelluti, S. Hernandez, M. Quaglio and C. F. Pirri, Phys. Chem. Chem. Phys., 2013, 15, 2596-2602.
- 91 H. Wang, H. Li, J. Wang, J. Wu, D. Li, M. Liu and P. Su, Electrochim. Acta, 2014, 137, 744-750.
- 92 M. M. Momeni, Rare Met., 2017, 36, 865-871.
- 93 J.-Y. Park, C.-S. Kim, K. Okuyama, H.-M. Lee, H.-D. Jang, S.-E. Lee and T. Kim, Copper and nitrogen doping on TiO₂ photoelectrodes and their functions in dye-sensitized solar cells, J. Power Sources, 2016.
- 94 S. Iwamoto, Y. Sazanami, M. Inoue, T. Inoue, T. Hoshi, K. Shigaki, M. Kaneko and A. Maenosono, ChemSusChem, 2008, 1, 401-403.
- 95 M. Nada, T. Gonda, Q. Shen, H. Shimada, T. Toyoda and N. Kobayashi, Jpn. J. Appl. Phys., 2009, 48, 025505.
- 96 M. Pan, H. Liu, Z. Yao and X. Zhong, J. Nanomater., 2015, 2015, 5.
- 97 T.-V. Nguyen, H.-C. Lee, M. A. Khan and O.-B. Yang, Sol. Energy, 2007, 81, 529-534.
- 98 H. Tian, L. Hu, C. Zhang, S. Chen, J. Sheng, L. Mo, W. Liu and S. Dai, J. Mater. Chem., 2011, 21, 863-868.
- 99 M. Wang, S. Bai, A. Chen, Y. Duan, Q. Liu, D. Li and Y. Lin, Electrochim. Acta, 2012, 77, 54-59.
- 100 T. Ma, M. Akiyama, E. Abe and I. Imai, Nano Lett., 2005, 5, 2543-2547.
- 101 H. Tian, L. Hu, C. Zhang, W. Liu, Y. Huang, L. Mo, L. Guo, J. Sheng and S. Dai, J. Phys. Chem. C, 2010, 114, 1627-1632.
- 102 Q. Sun, J. Zhang, P. Wang, J. Zheng, X. Zhang, Y. Cui, J. Feng and Y. Zhu, J. Renewable Sustainable Energy, 2012, 4, 023104.
- 103 B. Yacoubi, L. Samet, J. Bennaceur, A. Lamouchi and R. Chtourou, Properties of transition metal doped-titania electrodes: impact on efficiency of amorphous and nanocrystalline dye-sensitized solar cells, Mater. Sci. Semicond. Process., 2014, 30, 361-367.
- 104 R. Li, Y. Zhao, R. Hou, X. Ren, S. Yuan, Y. Lou, Z. Wang, D. Li and L. Shi, J. Photochem. Photobiol., A, 2016, 319-320, 62-69.
- 105 Y. Duan, N. Fu, Q. Liu, Y. Fang, X. Zhou, J. Zhang and Y. Lin, J. Phys. Chem. C, 2012, 116, 8888-8893.
- 106 W.-W. Xu, S.-Y. Dai, L.-H. Hu, L.-Y. Liang and K.-J. Wang, Chin. Phys. Lett., 2006, 23, 2288.
- 107 Z. Zhang, G. Li, Z. Cui, K. Zhang, Y. Feng and S. Meng, J. Solid State Chem., 2016, 237, 242-247.
- 108 L. Wei, Y. Yang, X. Xia, R. Fan, T. Su, Y. Shi, J. Yu, L. Li and Y. Jiang, RSC Adv., 2015, 5, 70512-70521.
- 109 J. C. Zhang, Z. Y. Han, Q. Y. Li, X. Y. Yang, Y. Yu and W. L. Cao, J. Phys. Chem. Solids, 2011, 72, 1239-1244.
- 110 Y. Jiang, Y. Chen, B. Zhang and Y. Feng, J. Electrochem. Soc., 2016, 163, F1133-F1138.
- 111 E. M. Jin, S. M. Jeong, H.-C. Kang and H.-B. Gu, ECS J. Solid State Sci. Technol., 2016, 5, Q109-Q114.
- 112 A. Ahmad, S. Buzby, C. Ni and S. I. Shah, J. Nanosci. Nanotechnol., 2008, 8, 2410-2418.

113 T. Bak, M. K. Nowotny, L. R. Sheppard and J. Nowotny, *J. Phys. Chem. C*, 2008, **112**, 12981–12987.

Nanoscale Advances

- 114 F. Giordano, A. Abate, J. P. Correa Baena, M. Saliba, T. Matsui, S. H. Im, S. M. Zakeeruddin, M. K. Nazeeruddin, A. Hagfeldt and M. Graetzel, *Nat. Commun.*, 2016, 7, 10379.
- 115 W. Guo, Y. Shen, L. Wu, Y. Gao and T. Ma, *J. Phys. Chem. C*, 2011, **115**, 21494–21499.
- 116 S. G. Ullattil, A. V. Thelappurath, S. N. Tadka, J. Kavil, B. K. Vijayan and P. Periyat, *Sol. Energy*, 2017, **155**, 490–495.
- 117 B. O'Regan and M. Gratzel, *Nature*, 1991, **353**, 737–740.
- 118 R. Amadelli, R. Argazzi, C. A. Bignozzi and F. Scandola, *J. Am. Chem. Soc.*, 1990, **112**, 7099–7103.
- 119 S. Ito, T. N. Murakami, P. Comte, P. Liska, C. Grätzel, M. K. Nazeeruddin and M. Grätzel, *Thin Solid Films*, 2008, 516, 4613–4619.
- 120 Y.-J. Chang, E.-H. Kong, Y.-C. Park and H. M. Jang, *J. Mater. Chem. A*, 2013, **1**, 9707–9713.
- 121 N. Mir and M. Salavati-Niasari, *Mater. Res. Bull.*, 2013, **48**, 1660–1667.
- 122 S. Iijima, Nature, 1991, 354, 56-58.
- 123 M. Law, L. E. Greene, J. C. Johnson, R. Saykally and P. Yang, *Nat. Mater.*, 2005, **4**, 455–459.
- 124 E. Enache-Pommer, J. E. Boercker and E. S. Aydil, *Appl. Phys. Lett.*, 2007, **91**, 123116.
- 125 J.-Y. Liao, B.-X. Lei, H.-Y. Chen, D.-B. Kuang and C.-Y. Su, *Energy Environ. Sci.*, 2012, **5**, 5750–5757.
- 126 X. Cai, H. Wu, S. Hou, M. Peng, X. Yu and D. Zou, *ChemSusChem*, 2014, 7, 474–482.
- 127 W. Liu, H. Lu, M. Zhang and M. Guo, *Appl. Surf. Sci.*, 2015, 347, 214–223.
- 128 X. Sheng, D. He, J. Yang, K. Zhu and X. Feng, *Nano Lett.*, 2014, 14, 1848–1852.
- 129 A. M. Bakhshayesh, M. R. Mohammadi, H. Dadar and D. J. Fray, *Electrochim. Acta*, 2013, **90**, 302–308.
- 130 D. K. Roh, W. S. Chi, S. H. Ahn, H. Jeon and J. H. Kim, *ChemSusChem*, 2013, **6**, 1384–1391.
- 131 Z.-j. Zhou, J.-q. Fan, X. Wang, W.-h. Zhou, Z.-l. Du and S.-x. Wu, *ACS Appl. Mater. Interfaces*, 2011, 3, 4349–4353.
- 132 C. Zha, L. Shen, X. Zhang, Y. Wang, B. A. Korgel, A. Gupta and N. Bao, *ACS Appl. Mater. Interfaces*, 2014, **6**, 122–129.
- 133 F.-T. Kong, S.-Y. Dai and K.-J. Wang, *Adv. OptoElectron.*, 2007, 2007, 13.
- 134 W.-Q. Wu, Y.-F. Xu, C.-Y. Su and D.-B. Kuang, *Energy Environ. Sci.*, 2014, 7, 644–649.
- 135 W.-Q. Wu, Y.-F. Xu, H.-S. Rao, C.-Y. Su and D.-B. Kuang, *J. Am. Chem. Soc.*, 2014, **136**, 6437–6445.
- 136 H. Li, Q. Yu, Y. Huang, C. Yu, R. Li, J. Wang, F. Guo, S. Jiao, S. Gao and Y. Zhang, ACS Appl. Mater. Interfaces, 2016, 8, 13384–13391.
- 137 Y.-C. Yen, P.-H. Chen, J.-Z. Chen, J.-A. Chen and K.-J. Lin, *ACS Appl. Mater. Interfaces*, 2015, 7, 1892–1898.
- 138 K.-W. Lee, M. Kim, J.-M. Kim, J. J. Kim and I.-H. Lee, *J. Alloys Compd.*, 2016, **656**, 568–572.
- 139 S. Jin, E. Shin and J. Hong, Nanomaterials, 2017, 7, 315.
- 140 E. Shin, S. Jin and J. Hong, *Appl. Surf. Sci.*, 2017, **416**, 353–357.

- 141 Z. Li, H. Yang, F. Wu, J. Fu, L. Wang and W. Yang, *Electron. Mater. Lett.*, 2017, **13**, 174–178.
- 142 G. Liu, H. Wang, M. Wang, W. Liu, R. E. Anugrah Ardhi, D. Zou and J. K. Lee, *Electrochim. Acta*, 2018, **267**, 34–40.
- 143 S. Ni, D. Wang, F. Guo, S. Jiao, Y. Zhang, J. Wang, B. Wang, L. Yuan, L. Zhang and L. Zhao, *J. Cryst. Growth*, 2019, 505, 62–68.
- 144 P. Makal and D. Das, ACS Omega, 2021, 6, 4362-4373.
- 145 P. Makal and D. Das, Mater. Chem. Phys., 2021, 266, 124520.
- 146 D. Jiang, Y. Hao, R. Shen, S. Ghazarian, A. Ramos and F. Zhou, ACS Appl. Mater. Interfaces, 2013, 5, 11906–11912.
- 147 J. Jiu, S. Isoda, F. Wang and M. Adachi, *J. Phys. Chem. B*, 2006, **110**, 2087–2092.
- 148 J. Jiu, F. Wang, S. Isoda and M. Adachi, *Chem. Lett.*, 2005, 34, 1506–1507.
- 149 L. De Marco, M. Manca, R. Giannuzzi, F. Malara, G. Melcarne, G. Ciccarella, I. Zama, R. Cingolani and G. Gigli, J. Phys. Chem. C, 2010, 114, 4228–4236.
- 150 H. Hafez, Z. Lan, Q. Li and J. Wu, *Nanotechnol., Sci. Appl.*, 2010, 3, 45.
- 151 K. Fan, W. Zhang, T. Peng, J. Chen and F. Yang, *J. Phys. Chem. C*, 2011, **115**, 17213–17219.
- 152 Q. Huang, G. Zhou, L. Fang, L. Hu and Z.-S. Wang, *Energy Environ. Sci.*, 2011, 4, 2145–2151.
- 153 F. Shao, J. Sun, L. Gao, S. Yang and J. Luo, *J. Phys. Chem. C*, 2011, **115**, 1819–1823.
- 154 J. Liu, Y. Wang and D. Sun, *Renewable Energy*, 2012, **38**, 214–218.
- 155 Z.-H. Liu, X.-J. Su, G.-L. Hou, S. Bi, Z. Xiao and H.-P. Jia, *J. Power Sources*, 2012, **218**, 280–285.
- 156 Y. Rui, Y. Li, Q. Zhang and H. Wang, *Nanoscale*, 2013, 5, 12574–12581.
- 157 H. Yu, J. Pan, Y. Bai, X. Zong, X. Li and L. Wang, *Chem.–Eur. J.*, 2013, **19**, 13569–13574.
- 158 W. Zhang, Y. Xie, D. Xiong, X. Zeng, Z. Li, M. Wang, Y.-B. Cheng, W. Chen, K. Yan and S. Yang, *ACS Appl. Mater. Interfaces*, 2014, **6**, 9698–9704.
- 159 J. Liu, J. Luo, W. Yang, Y. Wang, L. Zhu, Y. Xu, Y. Tang, Y. Hu, C. Wang and Y. Chen, *J. Mater. Sci. Technol.*, 2015, 31, 106–109.
- 160 S. Kathirvel, C. Su, Y.-J. Shiao, Y.-F. Lin, B.-R. Chen and W.-R. Li, *Sol. Energy*, 2016, 132, 310–320.
- 161 B. Liu and E. S. Aydil, *J. Am. Chem. Soc.*, 2009, **131**, 3985–3990.
- 162 T. Ohno, K. Sarukawa, K. Tokieda and M. Matsumura, Morphology of a TiO₂ Photocatalyst (Degussa, P-25) Consisting of Anatase and Rutile Crystalline Phases, J. Catal., 200, 203, 82–86.
- 163 M. Guli, Z. Hu, J. Yao, Z. Zhou, X. Sun and L. Chen, *Mater. Technol.*, 2017, 32, 239–244.
- 164 A. Hu, J. Wang, S. Qu, Z. Zhong, S. Wang and G. Liang, *J. Mater. Sci.: Mater. Electron.*, 2017, 28, 3415–3422.
- 165 M. Iraj, F. D. Nayeri, E. Asl-Soleimani and K. Narimani, *J. Alloys Compd.*, 2016, **659**, 44–50.
- 166 H.-Y. Chen, T.-L. Zhang, J. Fan, D.-B. Kuang and C.-Y. Su, *ACS Appl. Mater. Interfaces*, 2013, 5, 9205–9211.

167 F. Shao, J. Sun, L. Gao, J. Chen and S. Yang, RSC Adv., 2014, 4, 7805–7810.

- 168 W. Li, J. Yang, Q. Jiang, Y. Luo, Y. Hou, S. Zhou and Z. Zhou, *J. Power Sources*, 2015, **284**, 428–434.
- 169 H. Sayahi, K. Aghapoor, F. Mohsenzadeh, M. Mohebi Morad and H. R. Darabi, *Sol. Energy*, 2021, 215, 311–320.
- 170 S. Ghannadi, H. Abdizadeh, A. Rakhsha and M. R. Golobostanfard, *Mater. Chem. Phys.*, 2021, **258**, 123893.
- 171 S. Chatterjee, W. A. Webre, S. Patra, B. Rout, G. A. Glass, F. D'Souza and S. Chatterjee, *J. Alloys Compd.*, 2020, **826**, 154188.
- 172 V. S. Saji and M. Pyo, *Thin Solid Films*, 2010, **518**, 6542–6546.
- 173 K. Fujihara, A. Kumar, R. Jose, S. Ramakrishna and S. Uchida, *Nanotechnology*, 2007, **18**, 365709.
- 174 B. H. Lee, M. Y. Song, S.-Y. Jang, S. M. Jo, S.-Y. Kwak and D. Y. Kim, *J. Phys. Chem. C*, 2009, **113**, 21453–21457.
- 175 L. Yang and W. W. F. Leung, *Adv. Mater.*, 2013, **25**, 1792–1795.
- 176 H. Wang, Y. Bai, Q. Wu, W. Zhou, H. Zhang, J. Li and L. Guo, *Phys. Chem. Chem. Phys.*, 2011, **13**, 7008–7013.
- 177 W. Guo, C. Xu, X. Wang, S. Wang, C. Pan, C. Lin and Z. L. Wang, *J. Am. Chem. Soc.*, 2012, **134**, 4437–4441.
- 178 H. Wang, M. Liu, M. Zhang, P. Wang, H. Miura, Y. Cheng and J. Bell, *Phys. Chem. Chem. Phys.*, 2011, **13**, 17359–17366.
- 179 X. Gu, Y. Zhao and Y. Qiang, *J. Mater. Sci.: Mater. Electron.*, 2012, 23, 1373–1377.
- 180 Y. Zhao, X. Gu and Y. Qiang, *Thin Solid Films*, 2012, **520**, 2814–2818.
- 181 M. Ghaffari, M. B. Cosar, H. I. Yavuz, M. Ozenbas and A. K. Okyay, *Electrochim. Acta*, 2012, **76**, 446–452.
- 182 T. Yuan, H. Lu, B. Dong, L. Zhao, L. Wan, S. Wang and Z. Xu, *J. Mater. Sci.: Mater. Electron.*, 2015, **26**, 1332–1337.
- 183 Q. Yao, J. Liu, Q. Peng, X. Wang and Y. Li, *Chem.-Asian J.*, 2006, **1**, 737–741.
- 184 S.-M. Wang, W.-W. Dong, R.-H. Tao, Z.-H. Deng, J.-Z. Shao, L.-H. Hu, J. Zhu and X.-D. Fang, *J. Power Sources*, 2013, 235, 193–201.
- 185 X. Chen, Q. Du, W. Yang, W. Liu, Z. Miao and P. Yang, *J. Solid State Electrochem.*, 2018, **22**, 685–691.
- 186 N. Sriharan, T. S. Senthil, M. Kang and N. M. Ganesan, *Appl. Phys. A*, 2019, **125**, 118.
- 187 M. R. Subramaniam, D. Kumaresan, S. Jothi, J. D. McGettrick and T. M. Watson, *Appl. Surf. Sci.*, 2018, 428, 439–447.
- 188 A. Roy, S. Mukhopadhyay, P. S. Devi and S. Sundaram, *ACS Omega*, 2019, **4**, 1130–1138.
- 189 Y. Tang, C. Wang, Y. Hu, L. Huang, J. Fu and W. Yang, Superlattices Microstruct., 2016, 89, 1–6.
- 190 R. Jose, A. Kumar, V. Thavasi and S. Ramakrishna, *Nanotechnology*, 2008, **19**, 424004.
- 191 S. H. Kang, S. H. Choi, M. S. Kang, J. Y. Kim, H. S. Kim, T. Hyeon and Y. E. Sung, *Adv. Mater.*, 2008, **20**, 54–58.
- 192 Z. Wang, H. Wang, B. Liu, W. Qiu, J. Zhang, S. Ran, H. Huang, J. Xu, H. Han and D. Chen, ACS Nano, 2011, 5, 8412–8419.

- 193 M. Yang, B. Ding, S. Lee and J.-K. Lee, *J. Phys. Chem. C*, 2011, 115, 14534–14541.
- 194 G. K. Mor, O. K. Varghese, M. Paulose, K. Shankar and C. A. Grimes, Sol. Energy Mater. Sol. Cells, 2006, 90, 2011– 2075
- 195 Q. Zhou, Z. Fang, J. Li and M. Wang, *Microporous Mesoporous Mater.*, 2015, **202**, 22–35.
- 196 E. Ghadiri, N. Taghavinia, S. M. Zakeeruddin, M. Grätzel and J.-E. Moser, *Nano Lett.*, 2010, 10, 1632–1638.
- 197 J. R. Jennings, A. Ghicov, L. M. Peter, P. Schmuki and A. B. Walker, *J. Am. Chem. Soc.*, 2008, **130**, 13364–13372.
- 198 S. Li, Y. Liu, G. Zhang, X. Zhao and J. Yin, *Thin Solid Films*, 2011, **520**, 689–693.
- 199 P. Roy, S. Berger and P. Schmuki, *Angew. Chem., Int. Ed.*, 2011, **50**, 2904–2939.
- 200 A. Ghicov, S. P. Albu, R. Hahn, D. Kim, T. Stergiopoulos, J. Kunze, C.-A. Schiller, P. Falaras and P. Schmuki, *Chem.-Asian J.*, 2009, 4, 520–525.
- 201 S. H. Kang, J.-Y. Kim, Y. Kim, H. S. Kim and Y.-E. Sung, *J. Phys. Chem. C*, 2007, **111**, 9614–9623.
- 202 J. Wang and Z. Lin, Chem. Mater., 2009, 22, 579-584.
- 203 M. Adachi, Y. Murata, I. Okada and S. Yoshikawa, *J. Electrochem. Soc.*, 2003, **150**, G488–G493.
- 204 P. Maggie, S. Karthik, K. V. Oomman, K. M. Gopal and A. G. Craig, J. Phys. D: Appl. Phys., 2006, 39, 2498.
- 205 P. Roy, D. Kim, I. Paramasivam and P. Schmuki, *Electrochem. Commun.*, 2009, **11**, 1001–1004.
- 206 B.-X. Lei, J.-Y. Liao, R. Zhang, J. Wang, C.-Y. Su and D.-B. Kuang, J. Phys. Chem. C, 2010, 114, 15228–15233.
- 207 H. Park, W.-R. Kim, H.-T. Jeong, J.-J. Lee, H.-G. Kim and W.-Y. Choi, *Sol. Energy Mater. Sol. Cells*, 2011, **95**, 184–189.
- 208 Q. Zheng, H. Kang, J. Yun, J. Lee, J. H. Park and S. Baik, ACS Nano, 2011, 5, 5088–5093.
- 209 Z. Yi, Y. Zeng, H. Wu, X. Chen, Y. Fan, H. Yang, Y. Tang, Y. Yi, J. Wang and P. Wu, *Results Phys.*, 2019, 15, 102609.
- 210 Z. He, W. Que, P. Sun and J. Ren, *ACS Appl. Mater. Interfaces*, 2013, **5**, 12779–12783.
- 211 W.-Q. Wu, Y.-F. Xu, H.-S. Rao, C.-Y. Su and D.-B. Kuang, *J. Phys. Chem. C*, 2014, **118**, 16426–16432.
- 212 K. Gu, P. Zhong, M. Guo, J. Ma, Q. Jiang, S. Zhang, X. Zhou, Y. Xie, X. Ma and Y. Wang, *J. Solid State Electrochem.*, 2016, **20**, 3337–3348.
- 213 J.-H. Hu, S.-Q. Tong, Y.-P. Yang, J.-J. Cheng, L. Zhao and J.-X. Duan, *Acta Metall. Sin. (Engl. Lett.)*, 2016, **29**, 840–847.
- 214 W.-Y. Rho, M.-H. Chun, H.-S. Kim, H.-M. Kim, J. S. Suh and B.-H. Jun, *Nanomaterials*, 2016, **6**, 117.
- 215 N.-S. Peighambardoust, S. Khameneh-Asl and H. Azimi, *Appl. Phys. A*, 2017, **123**, 345.
- 216 M. Wu, J. Khan, J. Gu, S. He, X. Li, G. Ahmed, Z. Liu, M. N. Akhtar and W. Mai, *Nanoscale*, 2017.
- 217 V. Madurai Ramakrishnan, N. Muthukumarasamy, P. Balraju, S. Pitchaiya, D. Velauthapillai and A. Pugazhendhi, *Int. J. Hydrogen Energy*, 2020, 45, 15441– 15452.
- 218 X. Tang and D. Li, J. Phys. Chem. C, 2008, 112, 5405-5409.
- 219 J.-H. Kim, K. Zhu, Y. Yan, C. L. Perkins and A. J. Frank, *Nano Lett.*, 2010, **10**, 4099–4104.

Nanoscale Advances Review

- 220 Z. Hou, W. Que, J. Ren, Y. Xing, H. M. A. Javed, T. Zhou and L. Bing Kong, Ceram. Int., 2015, 41, S719-S724.
- 221 G. K. Mor, K. Shankar, M. Paulose, O. K. Varghese and C. A. Grimes, Nano Lett., 2006, 6, 215-218.
- 222 M. Yang, D. Kim, H. Jha, K. Lee, J. Paul and P. Schmuki, Chem. Commun., 2011, 47, 2032-2034.
- 223 S. So, K. Lee and P. Schmuki, Phys. Status Solidi Rapid Res. Lett., 2012, 6, 169-171.
- 224 A. Subramanian and H.-W. Wang, Appl. Surf. Sci., 2012, 258, 6479-6484.
- 225 J. Chen, M. Guo, H. Su, J. Zhang, L. Liu, H. Huang and K. Xie, J. Appl. Electrochem., 2018, 48, 1139-1149.
- 226 M. Guo, J. Chen, J. Zhang, H. Su, L. Liu, N. Fu and K. Xie, Electrochim. Acta, 2018, 263, 373-381.
- 227 N. Fu, X. Jiang, D. Chen, Y. Duan, G. Zhang, M. Chang, Y. Fang and Y. Lin, J. Power Sources, 2019, 439, 227076.
- 228 B. Bozkurt Çırak, Ç. Eden, Y. Erdoğan, Z. Demir, K. V. Özdokur, B. Caglar, S. Morkoç Karadeniz, T. Kılınç, A. Ercan Ekinci and Ç. Çırak, Optik, 2020, 203, 163963.
- 229 J. Wang, X. Nie, W. Wang, Z. Zhao, L. Li and Z. Zhang, Optik, 2021, 242, 167245.

- 230 K. Lee, R. Kirchgeorg and P. Schmuki, J. Phys. Chem. C, 2014, 118, 16562-16566.
- 231 S. So, A. Kriesch, U. Peschel and P. Schmuki, J. Mater. Chem. A, 2015, 3, 12603-12608.
- 232 W. Zhu, Y. Liu, A. Yi, M. Zhu, W. Li and N. Fu, Electrochim. Acta, 2019, 299, 339-345.
- 233 T. Lopez-Luke, A. Wolcott, L.-p. Xu, S. Chen, Z. Wen, J. Li, E. De La Rosa and J. Z. Zhang, J. Phys. Chem. C, 2008, 112, 1282-1292.
- 234 G. K. Mor, S. Kim, M. Paulose, O. K. Varghese, K. Shankar, J. Basham and C. A. Grimes, Nano Lett., 2009, 9, 4250-4257.
- 235 L. De Marco, M. Manca, R. Giannuzzi, M. R. Belviso, P. D. Cozzoli and G. Gigli, Energy Environ. Sci., 2013, 6, 1791-1795
- 236 K. Lee, A. Mazare and P. Schmuki, Chem. Rev., 2014, 114, 9385-9454.
- 237 R. P. Lynch, A. Ghicov and P. Schmuki, J. Electrochem. Soc., 2010, 157, G76.
- 238 S. G. Ullattil and P. Periyat, Sol. Energy, 2017, 147, 99-105.